3-D ERT FOR MONITORING OF INFILTRATING RIVER WATER

Published in *Geophysics*:

Coscia, I., Greenhalgh, S. A., Linde, N., Doetsch, J., Marescot, J., Günther, T., Vogt, T., and Green, A. G., 2011. 3D crosshole ERT for aquifer characterization and monitoring of infiltrating river water, *Geophysics*, **76**, G49-G59.

ABSTRACT

We are investigating the hydrogeological properties and hydrological responses of a productive aquifer in northeastern Switzerland. For this purpose we use 3-D crosshole electrical resistance tomography (ERT) to define the main lithological structures within the aquifer (through static inversion) and to monitor the water infiltration from an adjacent river. During precipitation events and subsequent river flooding, the river water resistivity increases. As a consequence, the electrical characteristics of the infiltrating water can be used as a natural tracer to delineate preferential flow paths and flow velocities. In this paper we focus primarily on the experiment installation, data collection strategy, the structural characterization of the site and give a brief overview of the ERT monitoring results. The monitoring system comprises 18 boreholes each equipped with 10 electrodes straddling the entire thickness of the gravel aquifer. A multichannel resistivity system programmed to cycle through various four-point electrode configurations of the 180 electrodes in a rolling sequence allows the measurement of approximately 15,500 apparent resistivity values every seven hours on a continuous basis. The 3-D static ERT inversion of data acquired under stable hydrological conditions provides a base model for future time-lapse inversion studies and the means to investigate the resolving capability of our acquisition scheme. In particular, it enables us to define the main lithological structures within the aquifer. The final ERT static model delineates a relatively high-resistivity low-porosity intermediate-depth layer throughout the investigated aquifer volume, consistent with results from well logging, and seismic and radar tomography models. The next step will be to define and implement an appropriate time-lapse ERT inversion scheme using the river water as a natural tracer. The main challenge will be to separate the superposed time-varying effects of water table height, temperature, and salinity variations associated with the infiltrating water.

A.1 INTRODUCTION

Electrical resistance tomography (ERT) is a popular subsurface imaging technique in hydrogeological, environmental, and civil engineering investigations [e.g., *Daily et al.*, 2005; *Kruse et al.*, 2006; *Robinson et al.*, 2008; *Sjödahl et al.*, 2009]. Crosshole implementations of the technique offer improved resolution and depth penetration over surface surveying [e.g., *Daily and Owen*, 1991; *Bing and Greenhalgh*, 2000; *Chambers et al.*, 2007]. Time-lapse studies, in which repeat measurements are made at different time intervals to track changes in the subsurface properties, have been performed for salt tracer experiments [*Slater et al.*, 2000;

Kemna et al., 2002; *Singha and Gorelick*; *Cassiani et al.*, 2006; *Wilkinson et al.*, 2010] and for the monitoring of steam injection [*Ramirez et al.*, 1993], environmental remediation [*Daily and Ramirez*, 1995; *LaBrecque et al.*, 1996a], biostimulation [*Lane et al.*, 2006], watershed characterization [*Miller et al.*, 2008] and various other processes [*Binley et al.*, 2002b; *Deiana et al.*, 2007; *Nimmer et al.*, 2007].

In this paper, we describe results of a novel 3-D crosshole resistivity monitoring experiment designed to investigate the hydrological properties and infiltration patterns of a producing gravel aquifer in direct connection with an adjacent river in northeastern Switzerland. Rainwater generally contains significantly lower concentrations of total dissolved solids (i.e., ions) than river water. As a consequence, strong precipitation in the catchment can cause the electrical resistivity of river water to increase. At our experimental site, high discharge events cause strong fluctuations of the river water electrical properties (increase in electrical resistivity). Therefore the river water which continuously infiltrates the aquifer can be used as a natural tracer to delineate the more hydraulically conductive sections of the aquifer and, as shown by *Cirpka et al.* [2007], to determine travel-time distributions.

Our research is part of a much larger project (RECORD - REstored CORridor Dynamics) aimed at assessing and modeling coupled hydrological, ecological, and biochemical effects of river restoration [*RECORD*, 2011]. In the project there are two study sites, one along a restored section (Neunforn) and one along an unrestored section (Widen) of the Thur River in Switzerland (Figure B1). Here, we restrict our attention to an initial hydrogeophysical study at the unrestored site. The eventual 4-D ERT model should provide new constraints for understanding interactions between the river and the connected aquifer. As summarized in the following paragraphs, our study differs from most earlier investigations in four ways: (1) the full 3-D inversion of an extensive crosshole data set acquired using electrodes deployed in a large number of boreholes, (2) an inversion strategy that accounts for surface and sediment layer topography, borehole inclinations, and the electrical properties of the borehole fluids, (3) the use of river water as a natural tracer to investigate an adjacent aquifer, and (4) continuously recorded data over a long time period at a sufficiently high sample rate to capture the transient process.

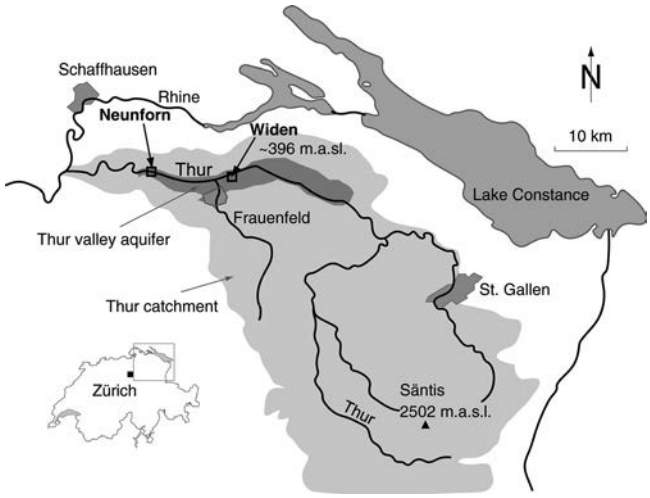

Figure B1. Location of the Thur catchment, Thur valley aquifer, and Nuenforn and Widen test sites in northeastern Switzerland. Modified from a figure prepared by Swisstopo (Swiss Federal Office of Topography).

ERT has previously been used for studying the interactions between rivers and their surroundings and for improving the modeling of fluvial systems. For example, *Crook et al.* [2008] used the technique to obtain information about the continuity and structure of stream-bed sediments. They employed information provided by a static resistivity model obtained from an ERT inversion of surface 2-D geoelectrical data. *Nyquist et al.* [2008] identified a zone of groundwater seepage into a river by combining the structural information about the site with that provided by the comparison of 2-D ERT images along the riverbed at low and high river stage conditions. Recently, *Ward et al.* [2010] investigated to what extent surface 2-D time-lapse ERT images, when combined with stream tracer experiments, can provide information about temporal and spatial dynamics in the hyporheic zone. Crosshole ERT, which is the basis of our work, usually yields more definitive information than surface ERT, especially if conducted in a time-lapse fashion. Previous such studies [e.g., *Singha and Gorelick*, 2005; *Slater and Binley*, 2006; *Kuras et al.*, 2009; *Müller et al.*, 2010; *Wilkinson et al.*, 2010], even if based on 3-D inversions, have generally involved sequential 2-D measurements only (i.e., between just one pair of boreholes at a time). Furthermore, the inversions have seldom been performed on data from more than four boreholes, because of the inability of standard inversion software to handle large 3-D data sets. In our study, we test a new acquisition and inversion strategy for carrying out a fully 3-D crosshole ERT experiment using electrodes located in 18 boreholes. We utilize a finite-element modeling (FEM) and inversion code based on unstructured meshes that allows us to incorporate typical

complexities associated with surface topography, sharp boundaries, and the boreholes themselves.

Most previous time-lapse ERT studies have been aimed at improving our understanding of subsurface solute transport by using time-varying electrical responses related to known injections of saline tracers into aquifers or known injections of water into the vadose zone [e.g., *Slater et al.*, 2000; *Singha and Gorelick*, 2005; *Slater and Binley*, 2006; *Müller et al.*, 2010; *Wilkinson et al.*, 2010]. Only a few studies have taken advantage of pre-existing electrical contrasts between the properties of subsurface fluids, such as those related to movements of contaminant plumes [*Slater and Sandberg*, 2000; *Nimmer et al.*, 2007] or those related to salt water - fresh water contacts within coastal aquifers [e.g., *Slater and Sandberg*, 2000; *Acworth and Dasey*, 2003; *de Franco et al.*, 2009; *Maurer et al.*, 2009; *Ogilvy et al.*, 2009]. In other investigations [e.g., *Hauck*, 2002; *Jayawickreme et al.*, 2008; *Yeh et al.*, 2008] natural occurring contrasts have been exploited. But as far as we know, no previous researchers have used the electrical properties of river water as a natural tracer to investigate aquifer response.

Time-lapse ERT usually involves frequently repeated measurements over a short period [e.g., *Wilkinson et al.*, 2010] or sparse measurements at infrequent intervals over a long period to determine seasonal variations in some property [e.g., *French and Binley*, 2004; *Hayley et al.*, 2009; *Krautblatter et al.*, 2010]. The present study is one of only a few examples (see also *de Franco et al.* [2009] and *Ogilvy et al.* [2009]) of a long-term ERT monitoring study (approximately one year of data have been collected in our case) with short-period data sampling (one data set of approximately 15,500 data points is acquired every 7 hours on a continual basis). This permits the investigation of aquifer infiltration and solute transport following river flooding events. It also enables us to investigate seasonal variations in electrical resistivity (e.g., same water height but different water resistivity due to snow melt, de-icing chemicals, or water temperature changes).

We begin by introducing the 18-borehole 180-electrode 3-D monitoring system and the geology of the site. Next, we describe the different electrode combinations and procedures used for remote data acquisition and then show the electrical signature of a typical flood event from the summer of 2009, which produces time-series of clear apparent resistivity anomalies. Finally, we present the results of a static 3-D ERT inversion for subsurface structure, incorporating various complexities such as surface and layer topography, decoupling of regularization across sharp layer boundaries, the borehole fluid effect, and borehole

deviations. Such 3-D images will be used as initial and reference models for future time-lapse inversion investigations.

A.2 WIDEN FIELD EXPERIMENT

A.2.1 Site description

The Widen study site (Figure B1) is located in northeastern Switzerland along the Thur River (a tributary of the Rhine River), which has a total length of approximately 127 km and a catchment area of approximately 1750 km². Due to the pre-alpine character of the upper Thur catchment that includes Mount Säntis (2502 m above sea level) and because of the absence of any natural or man-made reservoirs, the Thur River exhibits fluctuations in discharge and water table height similar to unregulated alpine rivers. Base flow has its maximum during snowmelt in spring, but flow peaks can occur at any time of the year in response to rainfall in the upper catchment (low discharge: 3 m^3/s; mean discharge: 20–50 m^3/s; peak discharge: up to 1000 m^3/s [*BAFU*, 2010]).

Our study site is located within the central Thur floodplain (altitude approximately 400 m above sea level, 2 km wide, and 30 km long), where the Thur River flows from east to west along the northern edge of a valley (Figure B1) that formed during the Pleistocene period by glaciers cutting into the underlying Tertiary bedrock. After the glaciers retreated, a lake was left behind and subsequently filled with fine silt and clay sediments were deposited in a lake. These sediments now constitute the aquitard at this location. The productive aquifer above the clay comprises a 6.5- to 7-m-thick layer of gravel and sand that is overlain by approximately 3 m of alluvial loam (see Figure B2b). During the 1890s, this area of the Thur River was channelized. The main channel is approximately 40 to 45 m wide. There is no overbank on the northern side because of a prominent hillslope that acts as a natural barrier at high discharge, whereas on the southern side there is a levee approximately 130 m from the river. Behind this levee, a side channel has been constructed to capture discharge from tributaries and drain the nearby agricultural land. There is a pumping well approximately 80 m from the levee that produces approximately 9000 m^3/d of drinking water for the 30,000 inhabitants of a nearby town (Frauenfeld in Figure B1).

At our local study site, the Thur River infiltrates year-round into the aquifer [*Cirpka et al.*, 2007], with a shallow local flow component at the top related to the infiltration of river water and a regional flow component in the lower sections following the main direction of the

valley. The overall direction of groundwater flow, influenced also by pumping well activity, is from northeast to southwest with fairly high velocities ranging between 1 and 50 m/day. The hydraulic conductivity of the aquifer is estimated from pumping and slug tests [*Diem et al.*, 2010] to range between 10^{-3} m/s and 10^{-2} m/s. Depending on the water table position, the aquifer displays unconfined and confined behavior.

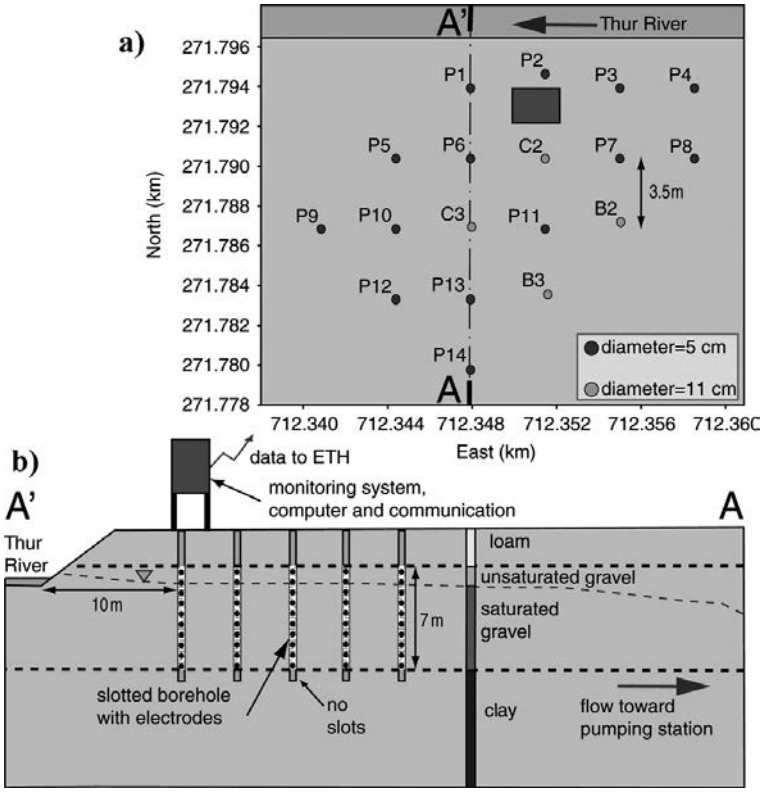

Figure B2. (a) Plan view of part of the Widen site showing borehole positions in Swiss grid coordinates with respect to the river and flood-proof hut (square). (b) Vertical section A' - A through the test site showing electrode installations, stratigraphy, groundwater table, and flow direction. Location of the section is shown in (a).

A.2.2 Experimental setup and field instrumentation

The main direction of groundwater flow, the hydrogeological parameters described in the previous section and surface ERT surveys to delineate the major vertical and horizontal resistivity variations at the site, guided the design of the electrical monitoring experiment. Eighteen boreholes at a nominal spacing of 3.5 m (Figure B2a) were installed with depths varying from 10 - 12 m. Four of them (B2, B3, C2, C3) are located at the corners of a square with 5 m side lengths and have 11 cm diameters to enable crosshole seismic and radar measurements to be made (Chapter 2) and to obtain samples in the coarse grain sedimentary

formation [*Diem et al.*, 2010]. The remaining 14 boreholes with 5 cm diameters were drilled using a direct-push machine. The entire borehole installation covers a surface area of 10 m × 15 m, which together with the 6.5 - 7 m thickness of the aquifer defines an investigation volume of approximately 1000 m^3. All 18 boreholes are lined with PVC or HPDE casing that is slotted along the aquifer section. (see Figure B2b). Each borehole contains 10 stainless steel cylindrical electrodes, spaced 0.7 m apart. The electrodes are each equipped with rubber disk packers fixed above and below (Figure B3c) to reduce as much as possible the vertical flow of water and partially focus the electric current flow outwards into the formation. The electrodes are connected via waterproof cables to the recording system (Figure B3d). The lowest 9 electrodes are usually below the water table, providing good electrical connection to the sedimentary formation through the borehole water and slotted casing. The top electrode can only be used when it makes electrical contact during periods of high water level.

A flood-proof hut at the site houses the recording system (Figures 2b and 3a and e) and provides access to mains power and a wireless link for data transmission to ETH Zurich. The resistivity instrument provides 10 channel recording capability and is interfaced to a switching unit that allows up to 192 electrodes to be connected and automatically selected according to a pre-determined sequence. Software is used to control the recording unit from a field computer also housed in the elevated flood-proof hut. It is possible to pre-program the sequence of measurements at user-defined timing intervals and to store the recorded voltage data (and other information, such as current strength, electrode geometry) directly on the PC hard disc. Wireless connection to the field computer enables the measurements to be controlled in real time and the data downloaded from the PC disc to a computer back at ETH Zürich for back up, quality control, and processing purposes.

Geophysical well logs (natural gamma, gamma-gamma, and neutron-neutron) run in each borehole define the gravel - clay interface in a more precise way than just using the disturbed cores retrieved during the borehole drilling campaign. The logs are useful in evaluating the static inversion model results. To reduce systematic errors associated with incorrect positions of the electrodes, the trajectories of each borehole were determined by a three-axis magnetometer and three-axis accelerometer downhole system. In addition to the electrodes, 14 multisensor devices and integrated data loggers are installed in 6 of the boreholes at different depths. These multisensors measure temperature, electrical conductivity, and hydraulic head of the groundwater every 15 minutes. This information will be vital for meaningful interpretations of the time-lapse ERT data.

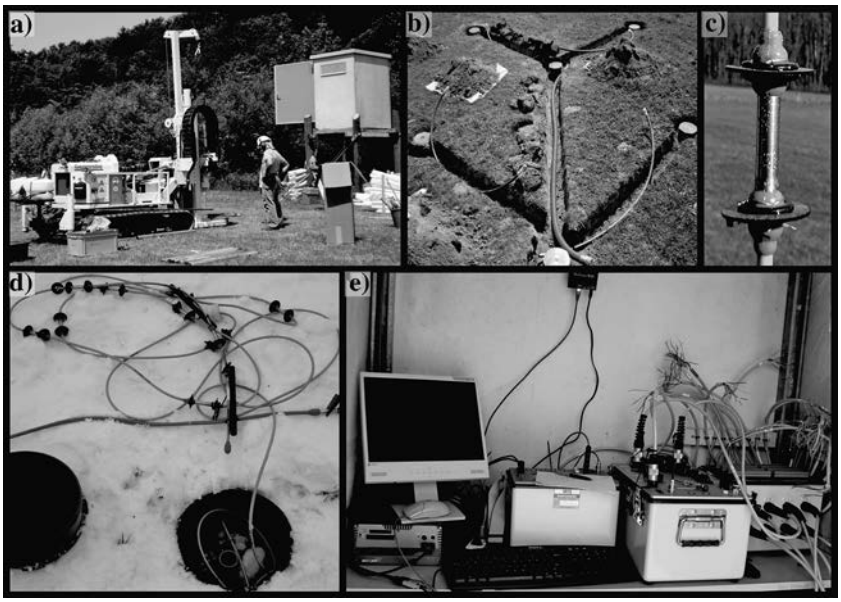

Figure B3. a) Direct-push drilling rig and, on the right, flood-proof hut. (b) Underground pipes connecting the geoelectric cables in the 18 boreholes with the measuring system inside the flood-proof hut. (c) Electrode with "packers". (d) Geoelectric cable equipped for a 5 cm borehole. (e) Field computer and components of the geoelectric acquisition system with a modem for wireless connection (top) inside the flood-proof hut.

A.2.3 ERT data collection scheme

To have a fast and fully 3-D data-capture sequence, we designed, after some preliminary synthetic studies and taking into account the borehole fluid effect (Chapter 4), a circulating four-point measurement scheme with the current and potential bipoles split between multiple boreholes. The data collection sequence operates as follows (Figure B4). One current electrode (A) occupies only one of 2 allowed positions in the 2 central boreholes C1 and C2 (i.e., the third electrode position in borehole C2 or the sixth electrode position in borehole C3 - see Figure B2 for the borehole locations), and the other current electrode (B) is always in the same borehole as one potential electrode (M). This second current electrode can be at any one of 3 different depths (counting from the top: the second, fifth, and eighth electrodes), whereas the potential electrode in the same hole moves through 3 other depths (counting from the top: the third, sixth, and ninth electrodes). Finally, the remaining potential electrode (N) scans all the positions in the boreholes immediately surrounding the one where the bipole BM is located (Figure B4b). This data collection scheme is repeated until all boreholes have been occupied once by the bipole BM and the remaining mobile potential electrode N has created all possible electrode combinations as described above (see Figure B4c).

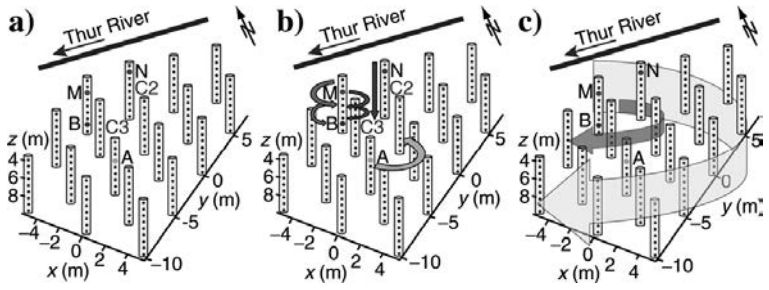

Figure B4. Illustration of how the configurations of the current electrodes A and B and potential electrodes M and N used in the geoelectric data acquisition system are circulated. (a) The 4 electrodes are always located in 3 different boreholes with A in only 2 possible positions in the two central boreholes. B and M always share a borehole and N is always in one of the boreholes immediately adjacent to them. (b) Movement of the electrodes is repeated for each borehole occupied by the current - potential (B - M) bipole. (c) Scheme repeated throughout the electrode array until the roving bipole has occupied all boreholes not occupied by the fixed current electrode.

This scheme is optimized to take advantage of the 10 independent channels of the recording system. A complete circulating sequence of approximately 15,500 data values (different electrode configurations across all 18 boreholes) is collected in 7 hours. The process is then repeated so that the aquifer is being continually monitored.

A.2.4 The river water as a natural electrical tracer

The hydrological regime of the Thur River is characterized by rapid undamped fluctuations of water level along its entire course after precipitation in the upper catchment. Associated with these fluctuations are significant changes to the electrical resistivity of the river water. As it infiltrates the aquifer, it acts as a resistivity anomaly that can be used as a natural tracer in time-lapse ERT imaging.

Figure B5 provides an example of the monitoring capability of the ERT system to track the magnitude and changing nature of this propagating resistivity anomaly. The presented data are for a flood event in the summer of 2009. When the river discharge increases, the river water resistivity increases. This can be readily observed by comparing the curve that represents the average water table height variation in the aquifer (Figure B5c) with the two curves that represent changes in water resistivity in the boreholes measured by the point loggers (Figure B5a). We show results from two loggers, one in borehole P3 close to the river and the other in borehole P12 some distance from the river (for locations see Figure B2a). Note the time delay between the peaks on the dotted and dashed curves (Figure B5a), clearly showing the transient nature of the infiltrating anomaly. It hits the borehole closest to the river

half a day earlier than that 15 m further away, and the signal magnitude is damped with increasing distance from the river. Figure B5a also shows the apparent resistivity time series (black circles) measured using the electrode configuration depicted in Figure B5b. This is a typical example of the ERT data trend during and following all flood events. The effect of the higher resistivity of the infiltrating water is readily apparent from the 15% anomaly over a period of several days

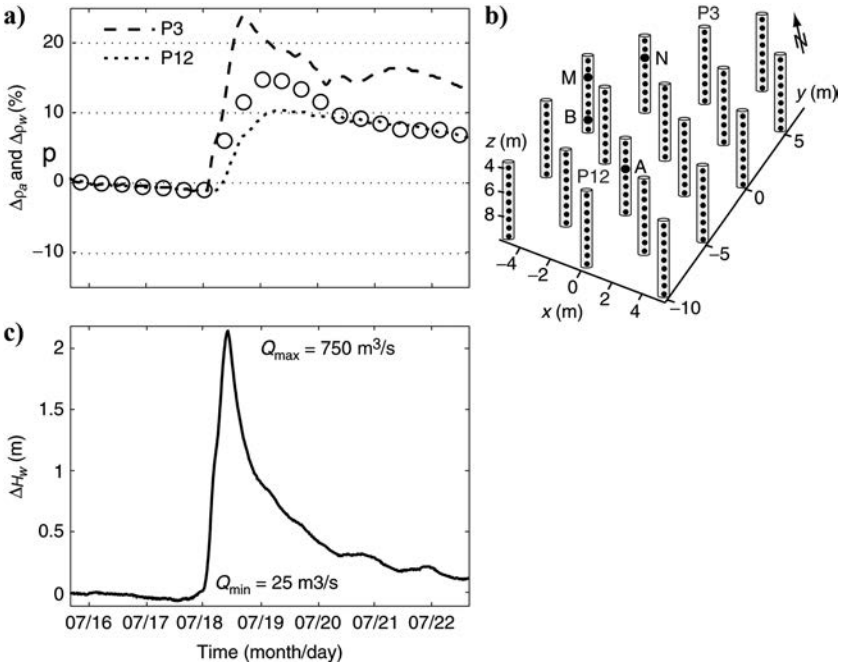

Figure B5. (a) Comparison between time series of relative apparent resistivity variations (black circles) during a strong hydrological event, and relative electrical-resistivity variations of the water at two locations (dotted and dashed curves - P3 and P12 near and far from the river, respectively). (b) ERT configuration used to record the apparent resistivity data shown in (a). (c) Mean variations of the water table position within the electrode array together with minimum and maximum discharges during the event.

A.3 FULL 3-D CROSSHOLE STATIC INVERSION

A.3.1 Static inversion approach and features

Our 3-D static inversions were performed using the open-source code BERT that is based on an unstructured finite-element framework [*Günther et al.*, 2006; *Rücker et al.*, 2006; www.resistivity.net]. It enabled all important aspects of the study site to be modeled in detail, including the surface topography, boreholes, and main geological boundaries (Figure B6).

The boreholes were explicitly modeled, taking into account their inclinations and declinations to correctly position all electrodes and reduce geometrical errors, which

otherwise could be significant (Figure B6b). Chapter 4 shows that the conductive borehole fluid has a strong effect on crosshole electric measurements for most standard AM-BN and AB-MN electrode configurations. They also demonstrated that this effect can be removed by explicitly including the boreholes in the modeling and inversion. This is especially important if the boreholes are closely spaced, the borehole diameters are large, and the resistivity contrasts between the fluid and host rock are high.

The overall stratigraphy at the site is well established. The approximate layer thicknesses are known from the boreholes and geophysical well logs, and the average layer resistivities are estimated from surface resistivity surveys. Under low river water conditions, the unsaturated part of the aquifer is approximately 1 m thick. It presents a significant resistivity contrast with the underlying saturated part of the aquifer that strongly influences the voltage measurements. As a consequence, the actual height of the water table should be determined from the borehole data loggers and fixed in the inversion, without imposing smoothness constraints (regularization) across what is known to be a sharp boundary (i.e., the very thin capillary fringe of gravel). From synthetic tests, we ascertain that the presence of the unsaturated gravel makes the sensitivities of the crosshole ERT measurements to the surface loam layer almost negligible. Therefore, the surface loam is not included in the initial model, allowing us to reduce slightly the number of inversion parameters. In analogy with the saturated - unsaturated interface, the clay - gravel interface is a boundary across which there is an order of magnitude resistivity contrast, such that it is desirable not to impose smoothness constraints across it.

The unsaturated and saturated zones of the aquifer, the gravel and clay layers, and the boreholes themselves constitute different regions in the inversion domain shown in Figure B6. This allows us to assign different initial values and different inversion parameters to each zone and to disconnect the regularization between the zones (see Table B1). A layered 1-D model of unsaturated gravel ($\rho_{m0} = 700$ Ωm) underlain sequentially by saturated gravel ($\rho_{m0} = 250$ Ωm) and clay ($\rho_{m0} = 25$ Ωm) constitutes a reasonable starting model for the inversions (Figures B2 and B6b).

The inversion domain (Figure B6b), in which the above-mentioned initial model is defined, is embedded within a much larger forward modeling domain (Figure B6a). The former is kept small to reduce the size of the inversion problem; it extends horizontally approximately 2 meters outward from the most external boreholes and vertically to include the unsaturated gravels and approximately 2 meters of the clayey aquitard (Figure B2b). The

latter needs to be large to avoid boundary effects and, for the same purpose, has internal boundaries controlled by mixed boundary conditions [*Günther et al.*, 2006]. At each iteration of the inversion routine, the resistivity values defined in the inversion domain are laterally extrapolated into the forward modeling domain.

The approximately 205,500 tetrahedra of the mesh for the inversion domain were generated using the meshing code Tetgen (http://tetgen.berlios.de). This code allowed different mesh properties to be defined in each region of the domain. To delineate the structures precisely, we imposed a maximum volume of 0.05 m^3 on all tetrahedra within the saturated aquifer (Figure B6b). The forward mesh created by the code BERT refined the inversion mesh [*Rücker et al.*, 2006] to have approximately 1,800,000 elements corresponding to approximately 300,000 nodes. Some of the cells (9%) were very small (less than 5 cm side length) in order to represent the boreholes around which abrupt resistivity changes occurred. Accordingly, singularity removal [*Blome et al.*, 2009] was not required. This was recognized after running several modeling and inversion tests, which demonstrated that the very fine mesh allowed the high potential gradients around the borehole sources to be accurately modeled.

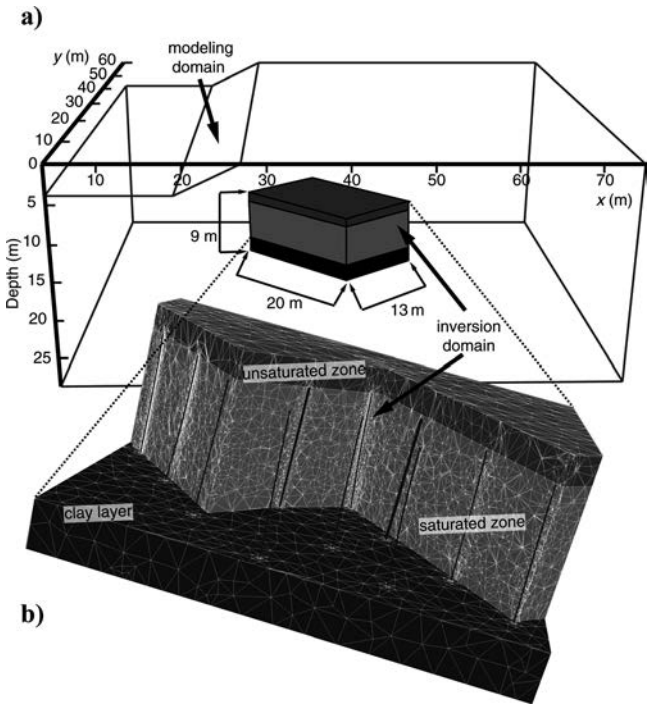

Figure B6. (a) Modeling domain with topography and the embedded inversion domain for the different regions (see Table B1), which shows the geometry of the input model for the inversion. (b) Unstructured parameter mesh, tilted boreholes and input topography of the saturated - unsaturated gravel and gravel - clay interfaces of the inversion domain.

We inverted for a logarithmic model function of the resistivity described as [*Günther*, 2004]:

$$m = \log(\rho - \rho_{lower}) - \log(\rho_{upper} - \rho), \quad \text{(B1)}$$

where ρ_{lower} and ρ_{upper} are lower and upper bounds defined for each region (see Table B1).

Within the aquifer, we employed anisotropic smoothing that penalized variations in the horizontal directions more than in the vertical direction to enhance the expected sub-horizontal layering in this region [see also *Linde et al.*, 2006a]. This was achieved by calculating a weighting factor W for the roughness matrix based on the vertical component of the normal vector n_z on each boundary between each tetrahedron of the mesh. The formulation for each tetrahedron boundary i is given by:

$$W_i = 1 + (w_z - 1) \cdot n_z, \quad \text{(B2)}$$

where w_z is a user-defined factor that can vary in each region of the model. This along with all other parameters used in each region of the inversion model are listed in Table B1.

The data set selected for determining a static 3-D resistivity model of the site was collected on 15 November 2009, during a period of stable hydrological conditions. The water level in the river was low and the groundwater table was approximately 4.2 m below the surface. Consequently, approximately 1 m of the aquifer was unsaturated. The approximately 22 Ωm electrical resistivity and approximately 8°C temperature of the water was similar on all the borehole sensors.

First we only considered configurations having electrode geometrical factors $K \leq$ +/- 1000, as a protection against probable low signal-to-noise data. Then, from the raw apparent resistivity data, we excluded all data values having standard deviations > 1% based on repeat measurements or voltages <1 mV. After that, we eliminated all data based on electrode configurations in which one or more of the electrodes were above the water table (i.e. those that had very high contact resistances). We also discarded all the negative apparent resistivities because of the limitation of the inversion code in handling negative values. Furthermore, we rejected any apparent resistivities greater than 500 Ωm or smaller than 30 Ωm. These upper and lower limits were set after first observing the frequency distribution (histogram) of apparent resistivities and considering the likely range of resistivities for saturated sandy gravel. Finally, approximately 12,000 data points (approximately 77% of the original data set) were used in an initial inversion aimed at defining the remaining outliers in the data set not removed in the previous data selection sequence (see later).

Finally, we apply an error model for weighting the data and the elements of the Jacobian matrix (sensitivities) during the inversion. The error (or uncertainty) for each voltage measurement is considered to consist of two parts [see *LaBrecque et al.*, 1996b]: a fixed absolute value of 0.1 mV (set by the instrument precision) and a relative error of 2% of the measured value (although we did experiment with other values in the range 1 - 4%). This yields an uncertainty of $\delta U=(0.1+0.02U)$ mV, where U is the recorded voltage in mV. When considering resistance or apparent resistivity as the input data, one should ideally take into account sources of errors related to the current strength and electrode positions, but these are judged to be much smaller than the voltage uncertainties. Moreover, the inversion code that we employ uses the logarithms of apparent resistivities $\log(\rho_a)$, rather than voltages or apparent resistivities themselves, therefore the estimated errors in these quantities used in data weighting matrix should be computed from the calculus of small changes (i.e., $\delta(\log(\rho_a))=\delta U / U=(0.1+0.02U) / U$). Although time consuming, we recalculate the Jacobian matrix (slightly less than 20 GB) after each iteration of the inversion and apply a robust reweighting of the data according to their misfit. For this reason, the initial median data error (2.02%) was, at the end of the inversion, slightly increased to 2.04%.

For all regions we apply a regularization parameter λ equal to 100 with an upscaled smoothness factor for the borehole region of the model (see Table B1). Tests were conducted with other λ values in the range 5 - 200. Conventional wisdom is to opt for the largest value consistent with being able to fit the data within a specified tolerance (say 2%). Smaller values of λ can introduce more detail in the model, some of which might be spurious, whereas overly large values yield excessively smooth models. We found that using values larger than 100 removed a small conductive feature that was independently known from the borehole logging [for further details about the error model and the choice of the regularization see also *Günther*, 2004].

After an initial inversion, we plotted the frequency distribution of data misfits and excluded those measurements lying outside a threshold given by 5 times the standard deviation of the distribution. The final data set, corresponding to almost 11,000 data points, was inverted using the same parameters as for the initial inversion. The inversion run time on a 2.66 GHz quad-core computer with 32 Gb of RAM was approximately 15 hours and it converged to the specified tolerance level ($\chi^2 = 1$) in 6 iterations.

Table B1. Inversion parameters used for each region of the model shown in Figure B7.

Region	Initial model resistivity ρ [Ωm]	Regularization type	Scaling factor n for the regularization parameter	Bounding values $\rho_{lower} - \rho_{upper}$ [Ωm]
Unsaturated gravel aquifer	700	Anisotropic smoothing ($w_z = 0.3$)	1	50 - 2000
Saturated gravel aquifer	250	Anisotropic smoothing ($w_z = 0.1$)	1	50 - 500
Aquitard (clay layer)	25	Anisotropic smoothing ($w_z = 0.3$)	1	5 - 45
Boreholes	22	Isotropic smoothing ($w_z = 1$)	10	10 - 50

A.3.2 Results

Figure B7 shows two vertical slices through the final 3-D model volume corresponding to the saturated part of the aquifer, one close and mainly parallel to the river (Figure B7a) and the other mainly along the principal diagonal (Figure B7b). The top and bottom layers (not shown) of the entire model correspond to the unsaturated gravel and the clay aquitard, respectively.

A central zone within the saturated gravel that is roughly 50 % more resistive (up to 320 Ωm) than the upper and lower parts (120 - 220 Ωm) is clearly delineated in the tomogram. It has an average thickness of approximately 2 m and lies in the 5 - 5.5 to 7 - 7.5 m depth range. It appears to be horizontal and continuous throughout the investigated volume. Earlier inversions, which were run without horizontal smoothing, show slightly inferior continuity of the resistive layer but still recover the layer.

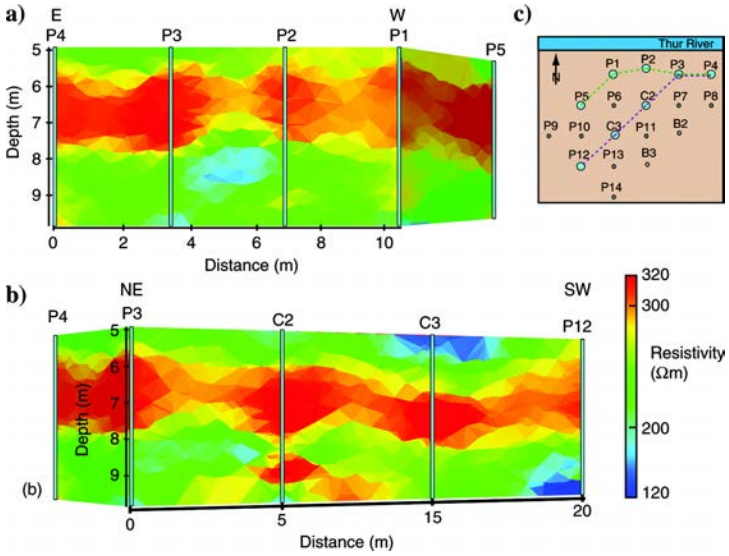

Figure B7. Resistivity cross sections extracted from the final inverted 3-D model viewed from the river looking to the (a) south (green dashed line) and (b) southeast (violet dashed line). (c) The locations of boreholes corresponding to the 2 slices in (a) and (b) are light blue.

In the plane containing the line of boreholes that lie close to the river (Figure B7a), the tomogram contains a more conductive zone (in blue) of approximately 1 m thickness. This zone is characterized by resistivities of approximately 130 Ωm. It corresponds to a lens of fine sediments observed in the drill core of nearby boreholes (P2 and P3). The resistive zone above this conductor appears less continuous, but this is probably caused by the resolution pattern in this area, which is strongly influenced by the presence of the conductive zone; being relatively conductive, the current is drawn into the zone, thereby decreasing current density and hence sensitivity elsewhere.

Further from the river, a decrease in the resistivity of the lower part of the aquifer is observed (Figure B7b). This could represent a higher percentage of fine material in proximity to the underlying clay.

A.4 DISCUSSION

A.4.1 Inversion aspects

The distances between the boreholes are rather small (3.5 m), such that any borehole deviations need to be considered. Given the maximum tilt of some boreholes (3^o), electrode mispositioning can be as much as 0.5 m if the boreholes are incorrectly assumed to be vertical. The tomograms would be adversely affected by such an error. We undertook some tests on a subset of data from 8 of the boreholes and found that the central more resistive layer within the aquifer becomes noticeably less continuous when the boreholes are taken to be uniformly vertical instead of slightly tilted.

Chapter 4 investigates the borehole fluid effect, whereby the resistivity contrast between the borehole fluid and host rock can introduce false structure in the medium after inversion if the boreholes are not explicitly modeled. We have established from a series of inversion tests that for the particular unconventional electrode configurations that we employed (see Section B.2.3) the borehole effect is minor. Very similar images (not shown) were obtained by ignoring the boreholes in the inversion process. This was partly a consequence of the relatively low resistivity contrast between the borehole fluid and the formation (8:1) and the fact that for most of the data collected with our unconventional configurations, the electrodes were placed in small diameter holes (5 cm); there would be significant artifacts in the images if classical electrode configurations (especially those having either the current electrodes or the potential electrodes in the same borehole) were to be employed, as in the study of Chapter

4. Inversions without including the boreholes require substantially fewer cells, thus reducing the memory requirements and the under-determined nature of the problem.

Another important technical consideration is decoupling the regularization across the layers and preserving the sharp boundaries where they are known to exist (e.g., at the water table and at the clay - gravel interface). This entails setting the weight of the individual model cells to zero in the presence of a known boundary, resulting in sharp gradients at this position. Failure to do so produces significant smearing and artifacts in the images. For example, since the clay is 10 times less resistive than the wet gravel, without layer decoupling the inversion produces an interface much shallower than that defined by the drill core and well-log data. This is illustrated in Figure B8, which shows inversion results along the section presented in Figure B7a adjacent to the river. The two plots correspond to inversions with (Figure B8a) and without (Figure B8b) decoupling the regularization between the layers. Notice the distortion of the clay interface and the disappearance of the low resistivity lens when no decoupling is applied. We performed several tests to confirm the importance of incorporating the correct positions of the known resistivity discontinuities. Surface topography should also, as a general rule, be incorporated in the inversion process, but from various synthetic tests we were able to establish that the zone of interest (saturated aquifer) is far enough away (i.e., at sufficient depth) that the measurements are only weakly sensitive to the sloping river bank topography.

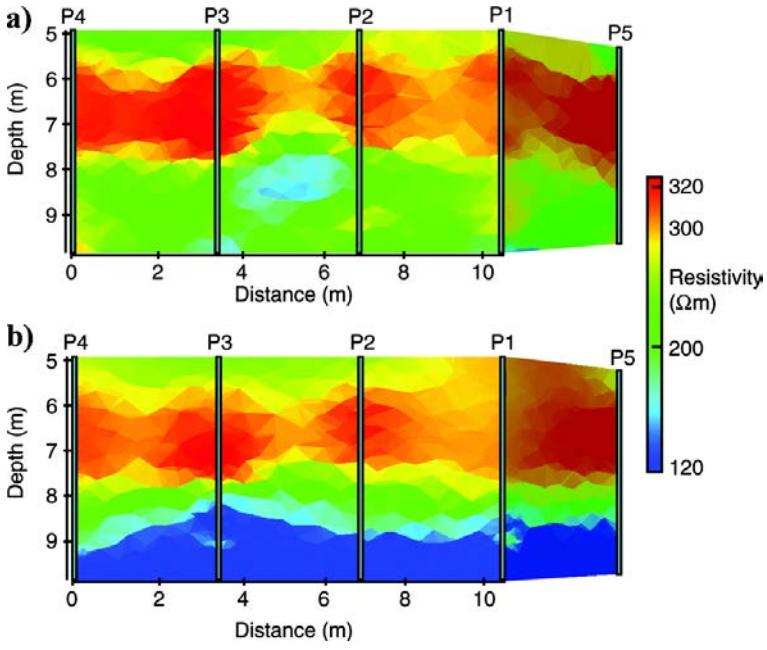

Figure B8. Cross sections extracted from inversion models in which the regularization between the layers is (a) decoupled (same as Figure B7a) and (b) not decoupled.

We have also compared our inversion model with that obtained at the site (Chapter 2) by jointly inverting seismic, radar, and ERT data sets acquired in the 11-cm-diameter boreholes (see Figure B2a for locations). The resistivity structures observed in the two studies were very similar.

A.4.2 Comparison between the inversion model and other data

Neutron-neutron, gamma-gamma, and natural-gamma well logs are available for all 18 boreholes. To compare the electrical variability of the aquifer with the well-log information, we compute average vertical resistivity profiles for each borehole. For this purpose, the average resistivity is calculated for a 40-cm-diameter 20-cm-high cylindrical volume centered about the borehole and about each point. Assuming that the highest number of counts of the neutron-neutron logs represents 50 % porosity and the lowest represents 12% porosity, corresponding to values estimated at the geologically similar Boise hydrogeophysical research site [*Barrash and Clemo*, 2002], the raw logs can be converted to approximate porosity estimates. The natural gamma log (not calibrated) gives information about the clay content [*Revil et al.*, 1998]. Figure B9 shows a comparison of the average vertical profile through the resistivity tomogram of borehole P3 with the relevant neutron-neutron (converted to porosity) and the natural gamma logs. The correlation coefficients between the average resistivity profile and well logs are -0.88 and -0.94, respectively. The central high resistivity zone of the aquifer has a relatively low porosity and low clay content (see also Chapter 2), whereas the lower resistivity region at the base of the aquifer is characterized by relatively high porosities and high clay content, consistent with the lens of fine sediments located in this depth range (see Figure B7a and Section B.3.2).

Electrical conductivity logs were also recorded at the site using a direct-push machine [*Schulmeister et al.*, 2003]. This system incorporated a Wenner array with an electrode spacing of 10 cm. The measurements were progressively made as the tool was hammered into the ground. Such resistivity logs were acquired at a total of 10 different locations between the boreholes. The instrument measured the average resistivity of the earth to a radius of approximately 10 cm (one third the current electrode spacing) centered about the borehole, whereas the vertical resolution was estimated to be approximately 10 cm. Measurements were taken at 2-3 cm depth intervals. Before each data set was acquired, the system was tested and calibrated. Figure B10 shows a representative vertical resistivity profile extracted from the inversion model at the same location where an electrical conductivity log was recorded. To be

comparable with the lower resolution ERT profile, the log data were averaged over 40-cm-depth intervals using a running average smoother. The trends of the two data sets are similar with a correlation coefficient of 0.73.

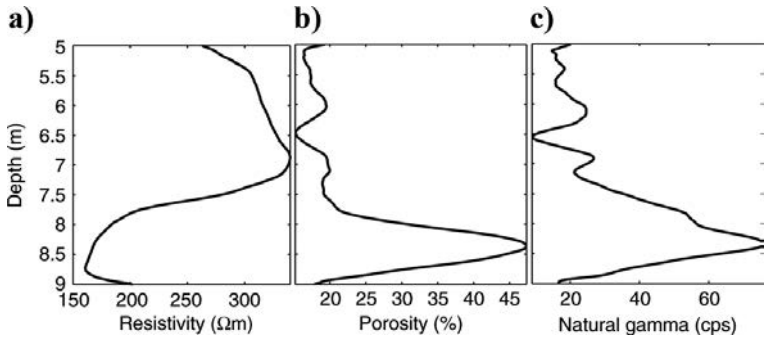

Figure B9. For borehole P3, comparison between vertical profiles of (a) resistivity extracted from the final inverted 3-D model around the borehole, (b) the neutron-neutron log converted to porosity, and (c) the natural gamma log.

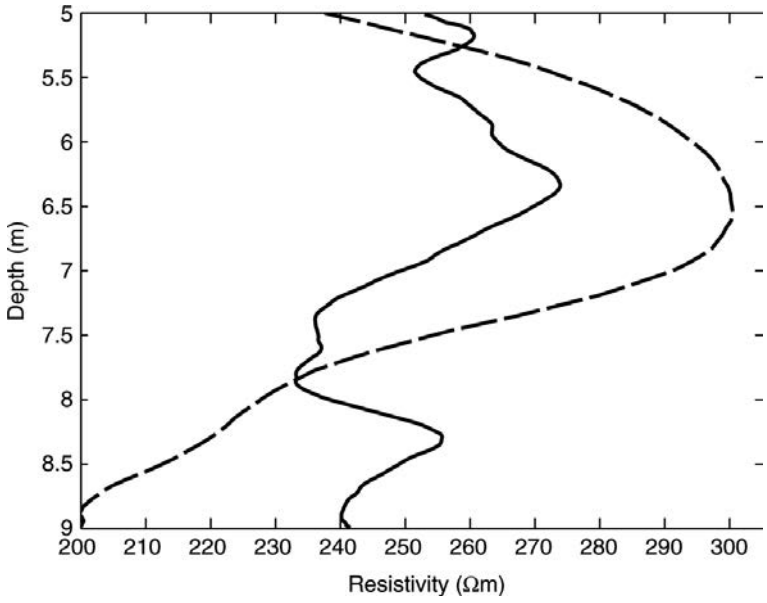

Figure B10. Example of a vertical resistivity profile extracted from the final ERT inversion model (dashed line) and a coincident resistivity log obtained with a Direct Push probe system (full line).

A.5 CONCLUSIONS

We have installed a resistivity monitoring system to study the hydrogeological properties of a gravel aquifer using flood events of an adjacent river as a natural electrical tracer. Eighteen boreholes equipped with total of 180 electrodes allow continuous collection of crosshole ERT measurements that can be used in both a static and dynamic sense to characterize the lithological sub-units and hydraulic properties of the aquifer. We utilize an unconventional fully 3-D data acquisition sequence that enables the collection of approximately 15,500 voltages (apparent resistivities) every 7 hours, of which roughly 11,000 are retained for the final inversions.

Approximately one year of ERT time series have now been acquired. They show the natural fluctuations of the water electrical properties of the adjacent infiltrating river. We have presented one example of a flood event, which produces a 15 % apparent resistivity anomaly, clearly showing how the geoelectrical data contain valuable information about the river infiltration process.

We have investigated problems related to inverting a very large static crosshole ERT data set. Disconnecting the regularization across the known sharp layer boundaries (water table and gravel - clay interface) and correct positioning of the electrodes were necessary to obtain meaningful results. Including the boreholes in the inversion (i.e., the borehole-fluid effect) would have avoided generating artifacts when using more classical electrode configurations. For the unconventional circulating 3-D electrode acquisition scheme employed in this study, we determined that the borehole-fluid effect was not significant. Accordingly, this scheme is a viable option when computing limitations are an issue or when unstructured FEM codes are unavailable.

The 3-D inversion of the chosen static ERT data set yielded a roughly 3-layer gravel aquifer model with superimposed minor variations. The central zone of the model, corresponding to roughly one third of the aquifer thickness, is 50 % more resistive than the upper and lower regions. The inverted model correlates with the geophysical well log data at the site. In particular, we observe strong correlations between the resistivity and neutron-neutron (representing porosity) and natural gamma (representing clay content) logs. From these comparisons, we interpret the relatively high-resistive central zone as being of lower porosity and the relatively low-resistive lower part of the aquifer as containing a larger proportion of fine sediments. These results are consistent with those previously obtained from

jointly inverted crosshole seismic, radar and ERT data acquired over a sub-volume of the experimental site.

This research forms the basis for future time-lapse ERT inversion that will be used to track preferential flow paths in the aquifer delineated by the infiltrating river water with different electrical properties and flow rates. A key challenge for the 4D imaging will be to separate the temporal effects of water table height, resistivity (salinity), and temperature variations. In fact, these three state variables, which are simultaneously sensed by the ERT data, can even have opposing effects on the data and make difficult the interpretation of the time-lapse results. To this end, we plan to investigate in detail the observed correlation between the input time series of the water height, resistivity and temperature in the river and the output ERT time series, and then filter the data in order to isolate the signal of interest related to the infiltrating less saline river water.

REFERENCES

Acworth, R. I., and Dasey, G. R., 2003. Mapping of the hyporheic zone around a tidal creek using a combination of borehole logging, borehole electrical tomography and cross-creek electrical imaging, New South Wales, Australia, *Hydrogeology Journal*, **11**, 368-377.

Ajo-Franklin, J. B., Minsley, B. J., and Daley, T. M., 2007. Applying compactness constraints to differential traveltime tomography, *Geophysics*, **72**, R67-R75.

al Hagrey, S. A., and Müller, C., 2000. GPR study of pore water content and salinity in sand, *Geophysical Prospecting*, **48**, 63-85.

Allègre, V., Jouniaux, L., Lehmann, F., and Sailhac, P., 2010. Streaming potential dependence on water-content in Fontainebleau sand, *Geophysical Journal International*, **182**, 1248-1266.

Alumbaugh, D., Chang, P. Y., Paprocki, L., Brainard, J. R., Glass, R. J., and Rautman, C. A., 2002. Estimating moisture contents in the vadose zone using cross-borehole ground penetrating radar: A study of accuracy and repeatability, *Water Resources Research*, **38**, 1309.

Alumbaugh, D. L., and Newman, G. A., 2000. Image appraisal for 2-D and 3-D electromagnetic inversion, *Geophysics*, **65**, 1455-1467.

Annan, A. P., 2005. GPR Methods for Hydrogeological Studies, in *Hydrogeophysics*, edited by Y. Rubin and S. S. Hubbard, pp. 185-213, Springer Netherlands.

Archie, G. E., 1942. The electrical resistivity log as an aid in determining some reservoir characteristics, *Transactions of the American institute of Mining, Metallurgical and Petroleum Engineers*, **146**, 54-62.

Arora, T., Linde, N., Revil, A., and Castermant, J., 2007. Non-intrusive characterization of the redox potential of landfill leachate plumes from self-potential data, *Journal of Contaminant Hydrology*, **92**, 274-292.

Aubert, M., and Yéené Atangana, Q., 1996. Self-potential method in hydrogeological exploration of volcanic areas, *Ground Water*, **34**, 1010-1016.

Avseth, P., Mukerji, T., Jørstad, A., Mavko, G., and Veggeland, T., 2001. Seismic reservoir mapping from 3-D AVO in a North Sea turbidite system, *Geophysics*, **66**, 1157-1176.

BAFU, 2010. Hydrologischer Atlas der Schweiz, *Bundeamt für Umwelt, Bern, Switzerland*.

Barrash, W., and Clemo, T., 2002. Hierarchical geostatistics and multifacies systems: Boise Hydrogeophysical Research Site, Boise, Idaho, *Water Resources Research*, **38**, 1196.

Barrenetxea, G., Ingelrest, F., Schaefer, G., and Vetterli, M., 2008. The hitchhiker's guide to successful wireless sensor network deployments, *Sensys'08: Proceedings of the 6th Acm Conference on Embedded Networked Sensor Systems*, 43-56.

Battin, T. J., and Sengschmitt, D., 1999. Linking sediment biofilms, hydrodynamics, and river bed clogging: Evidence from a large river, *Microbial Ecology*, **37**, 185-196.

Baumann, M., Jordan, P., Hoehn, E., and Geisser, H., 2009. Ein neues Grundwassermodell für das Thurtal, *Mitteilungen der Thurgauischen Naturforschenden Gesellschaft*, **63**.

Bedrosian, P. A., Maercklin, N., Weckmann, U., Bartov, Y., Ryberg, T., and Ritter, O., 2007. Lithology-derived structure classification from the joint interpretation of magnetotelluric and seismic models, *Geophysical Journal International*, **170**, 737-748.

Bélanger, C., Giroux, B., Gloaguen, E., and Lefebvre, R., 2010. GPR, ERT and CPT data integration for high resolution aquifer modeling, *13th International Conference on GPR*, 1-6.

Belghoul, A., 2007. *Caractérisation petrophysique et hydrodynamique du socle cristallin*: PhD thesis, University of Montpellier.

Belina, F. A., Ernst, J. R., and Holliger, K., 2009. Inversion of crosshole seismic data in heterogeneous environments: Comparison of waveform and ray-based approaches, *Journal of Applied Geophysics*, **68**, 85-94.

Bencala, K. E., 1984. Interactions of solutes and streambed sediment 2. A dynamic analysis of coupled hydrologic and chemical processes that determine solute transport, *Water Resources Research*, **20**, 1804-1814.

Beres, M., Green, A., Huggenberger, P., and Horstmeyer, H., 1995. Mapping the architecture of glaciofluvial sediments with 3-dimensional georadar, *Geology*, **23**, 1087-1090.

Beres, M., Huggenberger, P., Green, A. G., and Horstmeyer, H., 1999. Using two- and three-dimensional georadar methods to characterize glaciofluvial architecture, *Sedimentary Geology*, **129**, 1-24.

Bernhardt, E. S., Palmer, M. A., Allan, J. D., Alexander, G., Barnas, K., et al., 2005. Ecology - Synthesizing US river restoration efforts, *Science*, **308**, 636-637.

Beutel, J., Dyer, M., Lim, R., Plessl, C., Wohrle, M., et al., 2007. Automated wireless sensor network testing, *INSS 07: Proceedings of the Fourth International Conference on Networked Sensing Systems*, 303-303.

Beven, K., and Binley, A., 1992. The future of distributed models - model calibration and uncertainty prediction, *Hydrological Processes*, **6**, 279-298.

Bing, Z., and Greenhalgh, S. A., 1998a. A damping method for the computation of the 2.5-D Green's function for arbitrary acoustic media, *Geophysical Journal International*, **133**, 111-120.

Bing, Z., and Greenhalgh, S. A., 1998b. Crosshole acoustic velocity imaging with full-waveform spectral data: 2.5-D numerical simulations, *Exploration Geophysics*, **29**, 680-684.

Bing, Z., and Greenhalgh, S. A., 2000. Cross-hole resistivity tomography using different electrode configurations, *Geophysical Prospecting*, **48**, 887-912.

Binley, A., Winship, P., Middleton, R., Pokar, M., and West, J., 2001. High-resolution characterization of vadose zone dynamics using cross-borehole radar, *Water Resources Research*, **37**, 2639-2652.

Binley, A., Winship, P., West, L. J., Pokar, M., and Middleton, R., 2002a. Seasonal variation of moisture content in unsaturated sandstone inferred from borehole radar and resistivity profiles, *Journal of Hydrology*, **267**, 160-172.

Binley, A., Cassiani, G., Middleton, R., and Winship, P., 2002b. Vadose zone flow model parameterisation using cross-borehole radar and resistivity imaging, *Journal of Hydrology*, **267**, 147-159.

Binley, A., Cassiani, G., and Deiana, R., 2010. Hydrogeophysics: Opportunities and challenges, *Bollettino di Geofisica Teorica ed Applicata*, **51**, 267-284.

Birchak, J. R., Gardner, C. G., Hipp, J. E., and Victor, J. M., 1974. High dielectric constant microwave probes for sensing soil moisture, *Proceedings of the IEEE*, **62**, 93-98.

Bleistein, N., 1986. 2-1/2 dimensional inplane wave-propagation, *Geophysical Prospecting*, **34**, 686-703.

Blome, M., Maurer, H. R., and Schmidt, K., 2009. Advances in three-dimensional geoelectric forward solver techniques, *Geophysical Journal International*, **176**, 740-752.

Blome, M., Maurer, H., and Greenhalgh, S., 2011. Geoelectric experimental design - Efficient acquisition and exploitation of complete pole-bipole data sets, *Geophysics*, **76**, F15-F26.

Boggs, J. M., and Adams, E. E., 1992. Field study of dispersion in a heterogeneous aquifer: 4. Investigation of adsorption and sampling bias, *Water Resources Research*, **28**, 3325-3336.

Boggs, J. M., Young, S. C., Beard, L. M., Gelhar, L. W., Rehfeldt, K. R., and Adams, E. E., 1992. Field-study of dispersion in a heterogeneous aquifer: 1. Overview and site description, *Water Resources Research*, **28**, 3281-3291.

Bohlen, T., 2002. Parallel 3-D viscoelastic finite difference seismic modelling, *Computers & Geosciences*, **28**, 887-899.

Bolève, A., Revil, A., Janod, F., Mattiuzzo, J. L., and Fry, J. J., 2009. Preferential fluid flow pathways in embankment dams imaged by self-potential tomography, *Near Surface Geophysics*, **7**, 447-462.

Bosma, T. N. P., Ballemans, E. M. W., Hoekstra, N. K., teWelscher, R. A. G., Smeenk, J. G. M. M., et al., 1996. Biotransformation of organics in soil columns and an infiltration area, *Ground Water*, **34**, 49-56.

Bouman, C. A., 1997. Cluster: An unsupervised algorithm for modeling Gaussian mixtures, http://www.ece.purdue.edu/~bouman.

Bourg, A. C. M., and Bertin, C., 1993. Biogeochemical processes during the infiltration of river water into an alluvial aquifer, *Environmental Science & Technology*, **27**, 661-666.

Bouwer, H., and Rice, R. C., 1976. Slug test for determining hydraulic conductivity of unconfined aquifers with completely or partially penetrating wells, *Water Resources Research*, **12**, 423-428.

Bowling, J. C., Rodriguez, A. B., Harry, D. L., and Zheng, C., 2005. Delineating alluvial aquifer heterogeneity using resistivity and GPR data, *Ground Water*, **43**, 890-903.

Bowling, J. C., Harry, D. L., Rodriguez, A. B., and Zheng, C., 2007. Integrated geophysical and geological investigation of a heterogeneous fluvial aquifer in Columbus Mississippi, *Journal of Applied Geophysics*, **62**, 58-73.

Bradford, J. H., Clement, W. P., and Barrash, W., 2009. Estimating porosity with ground-penetrating radar reflection tomography: A controlled 3-D experiment at the Boise Hydrogeophysical Research Site, *Water Resources Research*, **45**, W00D26.

Brookes, A., 1988. *Channelized rivers: Prospectives for environmental management*, John Wiley and Sons, Chichester, UK.

Brovelli, A., and Cassiani, G., 2010. A combination of the Hashin-Shtrikman bounds aimed at modelling electrical conductivity and permittivity of variably saturated porous media, *Geophysical Journal International*, **180**, 225-237.

Brunke, M., and Gonser, T., 1997. The ecological significance of exchange processes between rivers and groundwater, *Freshwater Biology*, **37**, 1-33.

Butler, A. P., Mathias, S. A., Gallagher, A. J., Peach, D. W., and Williams, A. T., 2009. Analysis of flow processes in fractured chalk under pumped and ambient conditions (UK), *Hydrogeology Journal*, **17**, 1849-1858.

Butler, J. J., 1998. *The design, performance and analysis of slug tests*, Lewis, Boca Raton.

Butler, J. J., Garnett, E. J., and Healey, J. M., 2003. Analysis of slug tests in formations of high hydraulic conductivity, *Ground Water*, **41**, 620-630.

BUWAL, 2004. Wegleitung Grundwasserschutz, *Bundesamt für Umwelt, Wald und Landschaft, Bern, Switzerland*.

Carcione, J. M., Ursin, B., and Nordskag, J. I., 2007. Cross-property relations between electrical conductivity and the seismic velocity of rocks, *Geophysics*, **72**, E193-E204.

Cardenas, M. B., Wilson, J. L., and Zlotnik, V. A., 2004. Impact of heterogeneity, bed forms, and stream curvature on subchannel hyporheic exchange, *Water Resources Research*, **40**, W08307.

Cardenas, M. B., and Markowski, M. S., 2011. Geoelectrical imaging of hyporheic exchange and mixing of river water and groundwater in a large regulated river, *Environmental Science & Technology*, **45**, 1407-1411.

Carsel, R. F., and Parrish, R. S., 1988. Developing joint probability-distributions of soil-water retention characteristics, *Water Resources Research*, **24**, 755-769.

Caruthers, R. M., and Smith, I. F., 1992. The use of ground electrical survey methods for siting water-supply boreholes in shallow crystalline basement terrains, in *Hydrogeology of Crystalline Basement Aquifers in Africa*, edited by E. P. Wright and W. G. Burgess, pp. 203-220, Geological Society Special Publication.

Cassiani, G., Bruno, V., Villa, A., Fusi, N., and Binley, A. M., 2006. A saline trace test monitored via time-lapse surface electrical resistivity tomography, *Journal of Applied Geophysics*, **59**, 244-259.

Chambers, J. E., Wilkinson, P. B., Weller, A. L., Meldrum, P. I., Gilvy, R. D., and Caunt, S., 2007. Mineshaft imaging using surface and crosshole 3D electrical resistivity tomography: A case history from the East Pennine Coalfield, UK, *Journal of Applied Geophysics*, **62**, 324-337.

Chen, J. S., Hubbard, S., Rubin, Y., Murray, C., Roden, E., and Majer, E., 2004. Geochemical characterization using geophysical data and Markov Chain Monte Carlo methods: A case

study at the South Oyster bacterial transport site in Virginia, *Water Resources Research*, **40**, W12412.

Cirpka, O. A., Fienen, M. N., Hofer, M., Hoehn, E., Tessarini, A., et al., 2007. Analyzing bank filtration by deconvoluting time series of electric conductivity, *Ground Water*, **45**, 318-328.

Claerbout, J. F., and Muir, F., 1973. Robust modeling with erratic data, *Geophysics*, **38**, 826-844.

Constantz, J., Cox, M. H., and Su, G. W., 2003. Comparison of heat and bromide as ground water tracers near streams, *Ground Water*, **41**, 647-656.

Constantz, J., 2008. Heat as a tracer to determine streambed water exchanges, *Water Resources Research*, **44**, W00D10.

Coscia, I., Marescot, L., Maurer, H., Greenhalgh, S., and Linde, N., 2008. Experimental design for crosshole electrical resistivity tomography data sets, *14th Annual European Meeting of Environmental and Engineering Geophysics, EAGE.*

Coscia, I., Greenhalgh, S., Linde, N., Green, A., Günther, T., et al., 2010. A multi-borehole 3-D ERT monitoring system for aquifer characterization using river flood events as a natural tracer, *16th Annual European Meeting of Environmental and Engineering Geophysics, EAGE.*

Coscia, I., Greenhalgh, S. A., Linde, N., Doetsch, J., Marescot, L., et al., 2011a. 3D crosshole ERT for aquifer characterization and monitoring of infiltrating river water, *Geophysics*, **76**, G49-G59.

Coscia, I., Linde, N., Greenhalgh, S., Günther, T., and Green, A., 2011b. A deconvolution approach to correct time-lapse 3D ERT data and improve imaging of natural aquifer dynamics, *Water Resources Research*, under review.

Crook, N., Binley, A., Knight, R., Robinson, D. A., Zarnetske, J., and Haggerty, R., 2008. Electrical resistivity imaging of the architecture of substream sediments, *Water Resources Research*, **44**, W00D13.

Daily, W., and Owen, E., 1991. Cross-borehole resistivity tomography, *Geophysics*, **56**, 1228-1235.

Daily, W., Ramirez, A., Labrecque, D., and Nitao, J., 1992. Electrical resistivity tomography of vadose water movement, *Water Resources Research*, **28**, 1429-1442.

Daily, W., and Ramirez, A., 1995. Electrical-resistance tomography during in-situ trichloroethylene remediation at the savanna river site, *Journal of Applied Geophysics*, **33**, 239-249.

Daily, W., Ramirez, A., Binley, A., and LaBrecque, D., 2005. Electrical resistance tomography — theory and practice, in *Near surface geophysics*, edited by D. K. Butler, pp. 525-550, SEG.

Daniels, J. J., Allred, B., Binley, A., Labrecque, D., and Alumbaugh, D., 2005. Hydrogeophysical case studies in the vadose zone, in *Hydrogeophysics*, edited by Y. Rubin and S. S. Hubbard, pp. 413-440, Springer.

Darling, T., 2005. *Well logging and formation evaluation*, Elsevier.

Darnet, M., and Marquis, G., 2004. Modelling streaming potential (SP) signals induced by water movement in the vadose zone, *Journal of Hydrology*, **285**, 114-124.

Day-Lewis, F. D., Lane, J. W., Jr., Harris, J. M., and Gorelick, S. M., 2003. Time-lapse imaging of saline-tracer transport in fractured rock using difference-attenuation radar tomography, *Water Resources Research*, **39**, 1290.

Day-Lewis, F. D., and Lane, J. W., 2004. Assessing the resolution-dependent utility of tomograms for geostatistics, *Geophysical Research Letters*, **31**, L07503.

Day-Lewis, F. D., Singha, K., and Binley, A. M., 2005. Applying petrophysical models to radar travel time and electrical resistivity tomograms: Resolution-dependent limitations, *Journal of Geophysical Research-Solid Earth*, **110**, B08206.

Day-Lewis, F. D., Lane, J. W., and Gorelick, S. M., 2006. Combined interpretation of radar, hydraulic, and tracer data from a fractured-rock aquifer near Mirror Lake, New Hampshire, USA, *Hydrogeology Journal*, **14**, 1-14.

Day-Lewis, F. D., Chen, Y., and Singha, K., 2007. Moment inference from tomograms, *Geophysical Research Letters*, **34**, L22404.

de Franco, R., Biella, G., Tosi, L., Teatini, P., Lozej, A., et al., 2009. Monitoring the saltwater intrusion by time lapse electrical resistivity tomography: The Chioggia test site (Venice Lagoon, Italy), *Journal of Applied Geophysics*, **69**, 117-130.

Deiana, R., Cassiani, G., Kemna, A., Villa, A., Bruno, V., and Bagliani, A., 2007. An experiment of non-invasive characterization of the vadose zone via water injection and cross-hole time-lapse geophysical monitoring, *Near Surface Geophysics*, **5**, 183-194.

Dempster, A. P., Laird, N. M., and Rubin, D. B., 1977. Maximum likelihood from incomplete data via the EM algorithm, *Journal of the Royal Statistical Society, Series B (Methodological)*, **39**, 1-38.

Deutsch, C. V., and Journel, A. G., 1998. *GSLIB: Geostatistical software library and user's guide*, 2. edition ed., Oxford Univ. Press, New York, 2. edition.

Diem, S., Vogt, T., and Hoehn, E., 2010. Räumliche Charakterisierung der hydraulischen Leitfähigkeit in alluvialen Schotter-Grundwasserleitern: Ein Methodenvergleich, *Grundwasser*, **15**, 241-251.

Dietrich, C. R., and Newsam, G. N., 1997. Fast and exact simulation of stationary Gaussian processes through circulant embedding of the covariance matrix, *Siam Journal on Scientific Computing*, **18**, 1088-1107.

Dogan, M., Van Dam, R. L., Bohling, G. C., Butler, J. J., Jr., and Hyndman, D. W., 2011. Hydrostratigraphic analysis of the MADE site with full-resolution GPR and direct-push hydraulic profiling, *Geophysical Research Letters*, **38**, L06405.

Dorn, C., Linde, N., Le Borgne, T., Bour, O., and Baron, L., 2011. Single-hole GPR reflection imaging of solute transport in a granitic aquifer, *Geophysical Research Letters*, **38**, L08401.

Doussan, C., Jouniaux, L., and Thony, J. L., 2002. Variations of self-potential and unsaturated water flow with time in sandy loam and clay loam soils, *Journal of Hydrology*, **267**, 173-185.

EC, 2000. Directive 2000/60/EC of the European Parliament and of the council establishing a framework for community action in the field of water policy, *Official Journal of the European Community*, **L327**, 1-72.

Eckert, P., Lamberts, R., and Wagner, C., 2008. The impact of climate change on drinking water supply by riverbank filtration, *Water Science Technology*, **8**, 319-324.

Edmaier, K., Burlando, P., and Perona, P., 2011. Mechanisms of vegetation uprooting by flow in alluvial non-cohesive sediment, *Hydrology and Earth Systems Science Discussion*, **8**, 1365-1398.

Eisenberg, D., and Kauzmann, W., 1969. *The structure and properties of water*, Oxford University Press.

Ellis, R. G., and Oldenburg, D. W., 1994. Applied geophysical inversion, *Geophysical Journal International*, **116**, 5-11.

Eppstein, M. J., and Dougherty, D. E., 1998. Optimal 3-D traveltime tomography, *Geophysics*, **63**, 1053-1061.

Ernst, J. R., Maurer, H., Green, A. G., and Holliger, K., 2007a. Full-waveform inversion of crosshole radar data based on 2-D finite-difference time-domain solutions of Maxwell's equations, *Ieee Transactions on Geoscience and Remote Sensing*, **45**, 2807-2828.

Ernst, J. R., Green, A. G., Maurer, H., and Holliger, K., 2007b. Application of a new 2D time-domain full-waveform inversion scheme to crosshole radar data, *Geophysics*, **72**, J53-J64.

Ernst, J. R., 2007. *2-D finite-difference time-domain full-waveform inversion of crosshole georadar data*: PhD thesis, ETH Zurich.

Farquharson, C. G., 2008. Constructing piecewise-constant models in multidimensional minimum-structure inversions, *Geophysics*, **73**, K1-K9.

Favetto, A., Pomposiello, C., Booker, J., and Rossello, E. A., 2007. Magnetotelluric inversion constrained by seismic data in the Tucuman basin (Andean foothills, 27 degrees S, NW argentina), *Journal of Geophysical Research - Solid Earth*, **112**, B09104.

Fine, R. A., and Millero, F. J., 1973. Compressibility of water as a function of temperature and pressure, *Journal of Chemical Physics*, **59**, 5529-5536.

Fleckenstein, J. H., Niswonger, R. G., and Fogg, G. E., 2006. River-aquifer interactions, geologic heterogeneity, and low-flow management, *Ground Water*, **44**, 837-852.

Fournier, C., 1989. Spontaneous potentials and resistivity surveys applied to hydrogeology in a volcanic area - case-history of the Chaine-Des-Puys (Puy-De-Dome, France), *Geophysical Prospecting*, **37**, 647-668.

Fregoso, E., and Gallardo, L. A., 2009. Cross-gradients joint 3D inversion with applications to gravity and magnetic data, *Geophysics*, **74**, L31-L42.

French, H., and Binley, A., 2004. Snowmelt infiltration: Monitoring temporal and spatial variability using time-lapse electrical resistivity, *Journal of Hydrology*, **297**, 174-186.

Friedel, S., 2003. Resolution, stability and efficiency of resistivity tomography estimated from a generalized inverse approach, *Geophysical Journal International*, **153**, 305-316.

Friedel, S., Byrdina, S., Jacobs, F., and Zimmer, M., 2004. Self-potential and ground temperature at Merapi volcano prior to its crisis in the rainy season of 2000-2001, *Journal of Volcanology and Geothermal Research*, **134**, 149-168.

Füchtenbauer, H., 1988. *Sedimente und Sedimentgesteine: Sandsteine*, 4 ed., Schweizerbart, Stuttgart.

Gallardo, L. A., and Meju, M. A., 2003. Characterization of heterogeneous near-surface materials by joint 2D inversion of dc resistivity and seismic data, *Geophysical Research Letters*, **30**, 1658.

Gallardo, L. A., and Meju, M. A., 2004. Joint two-dimensional DC resistivity and seismic travel time inversion with cross-gradients constraints, *Journal of Geophysical Research - Solid Earth*, **109**, B03311.

Gallardo, L. A., Meju, M. A., and Pérez-Flores, M. A., 2005. A quadratic programming approach for joint image reconstruction: Mathematical and geophysical examples, *Inverse Problems*, **21**, 435-452.

Gallardo, L. A., 2007. Multiple cross-gradient joint inversion for geospectral imaging, *Geophysical Research Letters*, **34**, L19301.

Gallardo, L. A., and Meju, M. A., 2007. Joint two-dimensional cross-gradient imaging of magnetotelluric and seismic traveltime data for structural and lithological classification, *Geophysical Journal International*, **169**, 1261-1272.

Gallardo, L. A., and Meju, M. A., 2011. Structure-Coupled Multiphysics Imaging in Geophysical Sciences, *Reviews of Geophysics*, **49**, RG1003.

Garambois, S., Senechal, P., and Perroud, H., 2002. On the use of combined geophysical methods to assess water content and water conductivity of near-surface formations, *Journal of Hydrology*, **259**, 32-48.

Gasperikova, E., Zhang, Y., and Hubbard, S., 2008. Using self potential and multiphase flow modeling to optimize groundwater pumping*, EOS Transactions AGU, 89(53).*

Giannopoulos, A., 2005. Modelling ground penetrating radar by GprMax, *Construction and Building Materials*, **19**, 755-762.

Gibert, D., and Pessel, M., 2001. Identification of sources of potential fields with the continuous wavelet transform: Application to self-potential profiles, *Geophysical Research Letters*, **28**, 1863-1866.

Golub, G. H., and van Loan, C. F., 1996. *Matrix computations*, Johns Hopkins University Press.

Gooseff, M. N., Anderson, J. K., Wondzell, S. M., LaNier, J., and Haggerty, R., 2005. A modelling study of hyporheic exchange pattern and the sequence, size, and spacing of stream bedforms in mountain stream networks, Oregon, USA, *Hydrological Processes*, **19**, 2915-2929.

Grasmueck, M., 1996. 3-D ground-penetrating radar applied to fracture imaging in gneiss, *Geophysics*, **61**, 1050-1064.

Grinsted, A., Moore, J. C., and Jevrejeva, S., 2004. Application of the cross wavelet transform and wavelet coherence to geophysical time series, *Nonlinear Processes in Geophysics*, **11**, 561-566.

GschG, 1991. Gewaesserschutzgesetz,, *Bundesgesetz über den Schutz der Gewässer, Schweiz*, **814.20**, 30.

GSchV, 1998. Gewaesserschutzverordnung, *Bundesgesetz über den Schutz der Gewässer, Schweiz*, **814.201**, 60.

Günther, T., 2004. *Inversion methods and resolution analysis for the 2D/3D reconstruction of resistivity structures from DC measurements*, Ph.D. thesis thesis: TU Bergakademie Freiberg.

Günther, T., and Rücker, C., 2006. A general approach for introducing information into inversion and examples from dc resistivity inversion, in *14th Annual European Meeting of Environmental and Engineering Geophysics*, edited, p. P039, EAGE.

Günther, T., Rücker, C., and Spitzer, K., 2006. Three-dimensional modelling and inversion of dc resistivity data incorporating topography - II. Inversion, *Geophysical Journal International*, **166**, 506-517.

Günther, T., and Rücker, C., 2009. Advanced inversion strategies using a new geophysical inversion and modelling library, *15th Annual European Meeting of Environmental and Engineering Geophysics, EAGE.*

Haber, E., and Oldenburg, D., 1997. Joint inversion: A structural approach, *Inverse Problems*, **13**, 63-77.

Harbaugh, A. W., 2005. MODFLOW-2005, The U.S. Geological Survey modular ground-water model—the ground-water flow process, in *Book 6. Modeling techniques*, Ch. 16.

Harvey, J. W., and Bencala, K. E., 1993. The effect of streambed topography on surface-subsurface water exchange in mountain catchments, *Water Resources Research*, **29**, 89-98.

Hashin, Z., and Shtrikman, S., 1962. A variational approach to theory of effective magnetic permeability of multiphase materials, *Journal of Applied Physics*, **33**, 3125-&.

Hashin, Z., and Shtrikman, S., 1963. A variational approach to the theory of the elastic behaviour of multiphase materials, *Journal of the Mechanics and Physics of Solids*, **11**, 127-140.

Hatch, C. E., Fisher, A. T., Revenaugh, J. S., Constantz, J., and Ruehl, C., 2006. Quantifying surface water-groundwater interactions using time series analysis of streambed thermal records: Method development, *Water Resources Research*, **42**, W10410.

Hauck, C., 2002. Frozen ground monitoring using DC resistivity tomography, *Geophysical Research Letters*, **29**, 2016.

Hayley, K., Bentley, L. R., and Gharibi, M., 2009. Time-lapse electrical resistivity monitoring of salt-affected soil and groundwater, *Water Resources Research*, **45**.

Heinz, J., Kleineidam, S., Teutsch, G., and Aigner, T., 2003. Heterogeneity patterns of quaternary glaciofluvial gravel bodies (SW-Germany): Application to hydrogeology, *Sedimentary Geology*, **158**, 1-23.

Henderson, R. D., Day-Lewis, F. D., and Harvey, C. F., 2009. Investigation of aquifer-estuary interaction using wavelet analysis of fiber-optic temperature data, *Geophysical Research Letters*, **36**, L06403.

Hiscock, K. M., and Grischek, T., 2002. Attenuation of groundwater pollution by bank filtration, *Journal of Hydrology*, **266**, 139-144.

Hoehn, E., and Cirpka, O. A., 2006. Assessing residence times of hyporheic ground water in two alluvial flood plains of the Southern Alps using water temperature and tracers, *Hydrology and Earth System Sciences*, **10**, 553-563.

Hoehn, E., and Scholtis, A., 2011. Exchange between a river and groundwater, assessed with hydrochemical data, *Hydrology and Earth System Sciences*, **15**, 983-988.

Hollender, F., Tillard, S., and Corin, L., 1999. Multifold borehole radar acquisition and processing, *Geophysical Prospecting*, **47**, 1077-1090.

Holliger, K., Musil, M., and Maurer, H. R., 2001. Ray-based amplitude tomography for crosshole georadar data: A numerical assessment, *Journal of Applied Geophysics*, **47**, 285-298.

Hu, W. Y., Abubakar, A., and Habashy, T. M., 2009. Joint electromagnetic and seismic inversion using structural constraints, *Geophysics*, **74**, R99-R109.

Hubbard, S., and Linde, N., 2011. Hydrogeophysics, in *Treatise on water*, edited by P. Wilderer, Ch. 43, Elsevier.

Hubbard, S. S., Rubin, Y., and Majer, E., 1999. Spatial correlation structure estimation using geophysical and hydrogeological data, *Water Resources Research*, **35**, 1809-1825.

Hubbard, S. S., Chen, J. S., Peterson, J., Majer, E. L., Williams, K. H., et al., 2001. Hydrogeological characterization of the South Oyster Bacterial Transport Site using geophysical data, *Water Resources Research*, **37**, 2431-2456.

Huggenberger, P., 1993. Radar facies: Recognition of facies patterns and heterogeneities within Pleistocene Rhine gravels, NE Switzerland, *Geological Society, London, Special Publications*, **75**, 163-176.

Huggenberger, P., Hoehn, E., Beschta, R., and Woessner, W., 1998. Abiotic aspects of channels and floodplains in riparian ecology, *Freshwater Biology*, **40**, 407-425.

Hyndman, D. W., and Gorelick, S. M., 1996. Estimating lithologic and transport properties in three dimensions using seismic and tracer data: The Kesterson aquifer, *Water Resources Research*, **32**, 2659-2670.

Hyndman, D. W., and Harris, J. M., 1996. Traveltime inversion for the geometry of aquifer lithologies, *Geophysics*, **61**, 1728-1737.

Jackson, M. D., 2010. Multiphase electrokinetic coupling: Insights into the impact of fluid and charge distribution at the pore scale from a bundle of capillary tubes model, *Journal of Geophysical Research-Solid Earth*, **115**, B07206.

Jacobs, L. A., Vongunten, H. R., Keil, R., and Kuslys, M., 1988. Geochemical changes along a river-groundwater infiltration flow path - Glattfelden, Switzerland, *Geochimica Et Cosmochimica Acta*, **52**, 2693-2706.

Jakubowicz, H., 1990. A simple efficient method of dip-moveout correction, *Geophysical Prospecting*, **38**, 221-245.

Jardani, A., Revil, A., Boleve, A., Crespy, A., Dupont, J. P., et al., 2007. Tomography of the Darcy velocity from self-potential measurements, *Geophysical Research Letters*, **34**, L24403.

Jayawickreme, D. H., Van Dam, R. L., and Hyndman, D. W., 2008. Subsurface imaging of vegetation, climate, and root-zone moisture interactions, *Geophysical Research Letters*, **35**, L18404.

Jegen, M. D., Hobbs, R. W., Tarits, P., and Chave, A., 2009. Joint inversion of marine magnetotelluric and gravity data incorporating seismic constraints: Preliminary results of sub-basalt imaging off the Faroe Shelf, *Earth and Planetary Science Letters*, **282**, 47-55.

Jougnot, D., Ghorbani, A., Revil, A., Leroy, P., and Cosenza, P., 2010. Spectral induced polarization of partially saturated clay-rocks: A mechanistic approach, *Geophysical Journal International*, **180**, 210-224.

Jung, H. K., Min, D. J., Lee, H. S., Oh, S., and Chung, H., 2009. Negative apparent resistivity in dipole-dipole electrical surveys, *Exploration Geophysics*, **40**, 33-40.

Kalbus, E., Reinstorf, F., and Schirmer, M., 2006. Measuring methods for groundwater - surface water interactions: A review, *Hydrology and Earth System Sciences*, **10**, 873-887.

Kalbus, E., Schmidt, C., Molson, J. W., Reinstorf, F., and Schirmer, M., 2009. Influence of aquifer and streambed heterogeneity on the distribution of groundwater discharge, *Hydrology and Earth System Sciences*, **13**, 69-77.

Keery, J., Binley, A., Crook, N., and Smith, J. W. N., 2007. Temporal and spatial variability of groundwater-surface water fluxes: Development and application of an analytical method using temperature time series, *Journal of Hydrology*, **336**, 1-16.

Keller, G. V., and Frischknecht, F., 1966. *Electrical methods in geophysical prospecting*, Pergamon.

Kemna, A., Kulessa, B., and Vereecken, H., 2002. Imaging and characterisation of subsurface solute transport using electrical resistivity tomography (ERT) and equivalent transport models, *Journal of Hydrology*, **267**, 125-146.

Khalil, A. A., Stewart, R. R., and Henley, D. C., 1993. Full-wave-form processing and interpretation of kilohertz cross-well seismic data, *Geophysics*, **58**, 1248-1256.

Kipfer, R., Aeschbach-Hertig, W., Peeters, F., and Stute, M., 2002. Noble gases in lakes and ground waters, *Noble Gases in Geochemistry and Cosmochemistry*, **47**, 615-700.

Klotzsche, A., van der Kruk, J., Meles, G. A., Doetsch, J., Maurer, H., and Linde, N., 2010. Full-waveform inversion of cross-hole ground-penetrating radar data to characterize a gravel aquifer close to the Thur River, Switzerland, *Near Surface Geophysics*, **8**, 635-649.

Knight, R. J., and Nur, A., 1987. The dielectric-constant of sandstones, 60 Khz to 4 Mhz, *Geophysics*, **52**, 644-654.

Koch, K., Wenninger, J., Uhlenbrook, S., and Bonell, M., 2009. Joint interpretation of hydrological and geophysical data: Electrical resistivity tomography results from a process hydrological research site in the Black Forest Mountains, Germany, *Hydrological Processes*, **23**, 1501-1513.

Kondolf, G. M., 1998. Lessons learned from river restoration projects in California, *Aquatic Conservation-Marine and Freshwater Ecosystems*, **8**, 39-52.

Kosinski, W. K., and Kelly, W. E., 1981. Geoelectric soundings for predicting aquifer properties, *Ground Water*, **19**, 163-171.

Kowalsky, M. B., Finsterle, S., Peterson, J., Hubbard, S., Rubin, Y., et al., 2005. Estimation of field-scale soil hydraulic and dielectric parameters through joint inversion of GPR and hydrological data, *Water Resources Research*, **41**, W11425.

Krautblatter, M., Verleysdonk, S., Flores-Orozco, A., and Kemna, A., 2010. Temperature-calibrated imaging of seasonal changes in permafrost rock walls by quantitative electrical resistivity

tomography (Zugspitze, German/Austrian Alps), *Journal of Geophysical Research-Earth Surface*, **115**, F02003.

Kruse, S., Grasmueck, M., Weiss, M., and Viggiano, D., 2006. Sinkhole structure imaging in covered Karst terrain, *Geophysical Research Letters*, **33**, L16405.

Kumar, P., and Foufoula-Georgiou, E., 1997. Wavelet analysis for geophysical applications, *Reviews of Geophysics*, **35**, 385-412.

Kuras, O., Pritchard, J. D., Meldrum, P. I., Chambers, J. E., Wilkinson, P. B., et al., 2009. Monitoring hydraulic processes with automated time-lapse electrical resistivity tomography (ALERT), *Comptes Rendus Geoscience*, **341**, 868-885.

Kuroda, S., Takeuchi, M., and Kim, H. J., 2007. Full-waveform inversion algorithm for interpreting crosshole radar data: A theoretical approach, *Geosciences Journal*, **11**, 211-217.

LaBrecque, D. J., Ramirez, A. L., Daily, W. D., Binley, A. M., and Schima, S. A., 1996a. ERT monitoring on environmental remediation processes, *Measurement Science & Technology*, **7**, 375-383.

LaBrecque, D. J., Miletto, M., Daily, W., Ramirez, A., and Owen, E., 1996b. The effects of noise on Occam's inversion of resistivity tomography data, *Geophysics*, **61**, 538-548.

LaBrecque, D. J., and Yang, X., 2001. Difference inversion of ERT data: A fast inversion method for 3-D in situ monitoring, *Journal of Environmental and Engineering Geophysics*, **6**, 83-89.

Lacey, G., 1930. Stable channel in alluvium, *Proceedings of the Institution of Civil Engineers*, **229**, 259-292.

Lane, J. W., Day-Lewis, F. D., and Casey, C. C., 2006. Geophysical monitoring of a field-scale biostimulation pilot project, *Ground Water*, **44**, 430-443.

Langevin, C. D., Thorne, D. T., Jr., Dausman, A. M., Sukip, M. C., and Guo, W., 2008. SEAWAT version 4: A computer program for simulation of multi-species solute and heat transport, in *USGS Techniques and Methods Book 6*, Ch. A22.

Langevin, C. D., 2009. SEAWAT: A computer program for simulation of variable-density groundwater flow and multi-species solute and heat transport, *U.S. Geological Survey*, Fact Sheet 2009-3047.

Lanz, E., Boerner, D. E., Maurer, H., and Green, A., 1998. Landfill delineation and characterization using electrical, electromagnetic and magnetic methods, *Journal of Environmental and Engineering Geophysics*, **3**, 185-196.

Lazaratos, S. K., Harris, J. M., Rector, J. W., and Vanschaack, M., 1995. High-resolution crosswell imaging of a west texas carbonate reservoir 4. Reflection imaging, *Geophysics*, **60**, 702-711.

Le Borgne, T., Bour, O., Paillet, F. L., and Caudal, J. P., 2006. Assessment of preferential flow path connectivity, and hydraulic properties at single-borehole and cross-borehole scales in a fractured aquifer, *Journal of Hydrology*, **328**, 347-359.

Le Borgne, T., Bour, O., Riley, M. S., Gouze, P., Pezard, P. A., et al., 2007. Comparison of alternative methodologies for identifying and characterizing preferential flow paths in heterogeneous aquifers, *Journal of Hydrology*, **345**, 134-148.

Leonard, B. P., 1991. The ULTIMATE conservative difference scheme applied to unsteady one-dimensional advection, *Computer Methods in Applied Mechanics and Engineering*, **88**, 17-74.

Lesmes, D. P., and Friedman, S. P., 2005. Relationships between the electrical and hydrogeological properties of rocks and soils, in *Hydrogeophysics*, edited by Y. Rubin and S. S. Hubbard, pp. 87-128, Springer.

Li, S. H., Unsworth, M. J., Booker, J. R., Wei, W. B., Tan, H. D., and Jones, A. G., 2003. Partial melt or aqueous fluid in the mid-crust of Southern Tibet? Constraints from INDEPTH magnetotelluric data, *Geophysical Journal International*, **153**, 289-304.

Linde, N., Binley, A., Tryggvason, A., Pedersen, L. B., and Revil, A., 2006a. Improved hydrogeophysical characterization using joint inversion of cross-hole electrical resistance and ground-penetrating radar traveltime data, *Water Resources Research*, **42**, W12404.

Linde, N., Finsterle, S., and Hubbard, S., 2006b. Inversion of tracer test data using tomographic constraints, *Water Resources Research*, **42**, W04410.

Linde, N., Jougnot, D., Revil, A., Matthäi, S. K., Arora, T., et al., 2007a. Streaming current generation in two-phase flow conditions, *Geophysical Research Letters*, **34**, L03306.

Linde, N., and Revil, A., 2007. Inverting self-potential data for redox potentials of contaminant plumes, *Geophysical Research Letters*, **34**, L14302.

Linde, N., Revil, A., Bolève, A., Dagès, C., Castermant, J., et al., 2007b. Estimation of the water table throughout a catchment using self-potential and piezometric data in a Bayesian framework, *Journal of Hydrology*, **334**, 88-98.

Linde, N., Tryggvason, A., Peterson, J. E., and Hubbard, S. S., 2008. Joint inversion of crosshole radar and seismic traveltimes acquired at the South Oyster Bacterial Transport Site, *Geophysics*, **73**, G29-G37.

Linde, N., and Doetsch, J. A., 2010. Joint inversion of crosshole GPR and seismic traveltime data, in *Advances in near-surface seismology and ground-penetrating radar*, edited by R. D. Miller, J. H. Bradford and K. Holliger, Ch. 1, pp. 1-18, Society of Exploration Geophysicists.

Linde, N., Doetsch, J., Jougnot, D., Genoni, O., Dürst, Y., et al., 2011. Self-potential investigations of a gravel bar in a restored river corridor, *Hydrology and Earth System Sciences*, **15**, 729-742.

Lines, L. R., Schultz, A. K., and Treitel, S., 1988. Cooperative inversion of geophysical data, *Geophysics*, **53**, 8-20.

Loke, M. H., and Barker, R. D., 1996. Practical techniques for 3D resistivity surveys and data inversion, *Geophysical Prospecting*, **44**, 499-523.

Long, J. C. S., Aydin, A., Brown, S. R., Einstein, H. H., Hestir, K., et al., 1996. *Rock fracture and fluid flow: Contemporary understanding and applications*, National Academy Press, Washington, DC.

Looms, M. C., Jensen, K. H., Binley, A., and Nielsen, L., 2008. Monitoring unsaturated flow and transport using cross-borehole geophysical methods, *Vadose Zone Journal*, **7**, 227.

Lowry, T., Allen, M. B., and Shive, P. N., 1989. Singularity removal: A refinement of resistivity modeling techniques, *Geophysics*, **54**, 766-774.

Lunt, I. A., Bridge, J. S., and Tye, R. S., 2004. A quantitative three-dimensional depositional model of gravelly braided rivers, *Sedimentology*, **51**, 1155-1155.

Maineult, A., Bernabe, Y., and Ackerer, P., 2004. Electrical response of flow, diffusion, and advection in a laboratory sand box, *Vadose Zone Journal*, **3**, 1180-1192.

Maineult, A., Bernabe, Y., and Ackerer, P., 2005. Detection of advected concentration and pH fronts from self-potential measurements, *Journal of Geophysical Research-Solid Earth*, **110**, B11205.

Maineult, A., Strobach, E., and Renner, J., 2008. Self-potential signals induced by periodic pumping tests, *Journal of Geophysical Research-Solid Earth*, **113**, B01203.

Mair, J. A., and Green, A. G., 1981. High-resolution seismic-reflection profiles reveal fracture-zones within a homogeneous granite batholith, *Nature*, **294**, 439-442.

Maraun, D., and Kurths, J., 2004. Cross wavelet analysis: Significance testing and pitfalls, *Nonlinear Processes in Geophysics*, **11**, 505-514.

Marescot, L., Rigobert, S., P. Lopes, S., Lagabrielle, R., and Chapellier, D., 2006. A general approach for DC apparent resistivity evaluation on arbitrarily shaped 3D structures, *Journal of Applied Geophysics*, **60**, 55-67.

Maurer, H., Holliger, K., and Boerner, D. E., 1998. Stochastic regularization: Smoothness or similarity?, *Geophysical Research Letters*, **25**, 2889-2892.

Maurer, H., and Musil, M., 2004. Effects and removal of systematic errors in crosshole georadar attenuation tomography, *Journal of Applied Geophysics*, **55**, 261-270.

Maurer, H., and Friedel, S., 2006. Outer-space sensitivities in geoelectrical tomography, *Geophysics*, **71**, G93-G96.

Maurer, H., Friedel, S., and Jaeggi, D., 2009. Characterization of a coastal aquifer using seismic and geoelectric borehole methods, *Near Surface Geophysics*, **7**, 353-366.

Mazac, O., Kelly, W. E., and Landa, I., 1987. Surface geoelectrics for groundwater pollution and protection studies, *Journal of Hydrology*, **93**, 277-294.

McClymont, A. F., Green, A. G., Streich, R., Horstmeyer, H., Tronicke, J., et al., 2008. Visualization of active faults using geometric attributes of 3D GPR data: An example from the Alpine Fault Zone, New Zealand, *Geophysics*, **73**, B11-B23.

McElwee, C. D., and Zenner, M. A., 1998. A nonlinear model for analysis of slug-test data, *Water Resources Research*, **34**, 55-66.

Meles, G. A., Van der Kruk, J., Greenhalgh, S. A., Ernst, J. R., Maurer, H., and Green, A. G., 2010. A new vector waveform inversion algorithm for simultaneous updating of conductivity and permittivity parameters from combination crosshole/borehole-to-surface GPR data, *Ieee Transactions on Geoscience and Remote Sensing*, **48**, 3391-3407.

Merkli, B., 1975. *Untersuchungen über Mechanismen und Kinetik der Elimination von Bakterien und Viren im Grundwasser*: ETH Zurich.

Miall, A. D., 1995. Description and interpretation of fluvial deposits - A critical perspective, *Sedimentology*, **42**, 379-384.

Michel, S., Salehi, A., Luo, L., Dawes, N., Aberer, K., et al., 2009. Environmental monitoring 2.0, *Icde: 2009 Ieee 25th International Conference on Data Engineering, Vols. 1-3*, 1507-1510.

Michot, D., Benderitter, Y., Dorigny, A., Nicoullaud, B., King, D., and Tabbagh, A., 2003. Spatial and temporal monitoring of soil water content with an irrigated corn crop cover using surface electrical resistivity tomography, *Water Resources Research*, **39**, 1138.

Miller, C. R., Routh, P. S., Brosten, T. R., and McNamara, J. P., 2008. Application of time-lapse ERT imaging to watershed characterization, *Geophysics*, **73**, G7-G17.

Minsley, B. J., 2007. *Modeling and inversion of self-potential data*: PhD thesis, Massachusetts Institute of Technology.

Minsley, B. J., Sogade, J., and Morgan, F. D., 2007. Three-dimensional source inversion of self-potential data, *Journal of Geophysical Research*, **112**.

Mitchell, T. M., 1997. *Machine learning*, McGraw-Hill, New York.

Monego, M., Cassiani, G., Deiana, R., Putti, M., Passadore, G., and Altissimo, L., 2010. A tracer test in a shallow heterogeneous aquifer monitored via time-lapse surface electrical resistivity tomography, *Geophysics*, **75**, WA61-WA73.

Monteiro Santos, F. A., Sultan, S. A., Represas, P., and El Sorady, A. L., 2006. Joint inversion of gravity and geoelectrical data for groundwater and structural investigation: Application to the northwestern part of Sinai, Egypt, *Geophysical Journal International*, **165**, 705-718.

Mora, P., 1987. Nonlinear two-dimensional elastic inversion of multioffset seismic data, *Geophysics*, **52**, 1211-1228.

Müller, K., Vanderborght, J., Englert, A., Kemna, A., Huisman, J. A., et al., 2010. Imaging and characterization of solute transport during two tracer tests in a shallow aquifer using electrical resistivity tomography and multilevel groundwater samplers, *Water Resources Research*, **46**, W03502.

Musil, M., Maurer, H. R., and Green, A. G., 2003. Discrete tomography and joint inversion for loosely connected or unconnected physical properties: Application to crosshole seismic and georadar data sets, *Geophysical Journal International*, **153**, 389-402.

Nadeau, D. F., Brutsaert, W., Parlange, M. B., Bou-Zeid, E., Barrenetxea, G., et al., 2009. Estimation of urban sensible heat flux using a dense wireless network of observations, *Environmental Fluid Mechanics*, **9**, 635-653.

Nimmer, R. E., Osiensky, J. L., Binley, A. M., Sprenke, K. F., and Williams, B. C., 2007. Electrical resistivity imaging of conductive plume dilution in fractured rock, *Hydrogeology Journal*, **15**, 877-890.

Nimmer, R. E., Osiensky, J. L., Binley, A. M., and Williams, B. C., 2008. Three-dimensional effects causing artifacts in two-dimensional, cross-borehole, electrical imaging, *Journal of Hydrology*, **359**, 59-70.

Nyquist, J. E., Freyer, P. A., and Toran, L., 2008. Stream bottom resistivity tomography to map ground water discharge, *Ground Water*, **46**, 561-569.

Ogilvy, R. D., Meldrum, P. I., Kuras, O., Wilkinson, P. B., Chambers, J. E., et al., 2009. Automated monitoring of coastal aquifers with electrical resistivity tomography, *Near Surface Geophysics*, **7**, 367-375.

Oldenburg, D. W., and Li, Y. G., 1999. Estimating depth of investigation in dc resistivity and IP surveys, *Geophysics*, **64**, 403-416.

Olsson, O., Falk, L., Forslund, O., Lundmark, L., and Sandberg, E., 1992. Borehole radar applied to the characterization of hydraulically conductive fracture-zones in crystalline rock, *Geophysical Prospecting*, **40**, 109-142.

Oreskes, N., Shrader-Frechette, K., and Belitz, K., 1994. Verification, validation, and confirmation of numerical models in the earth sciences, *Science*, **263**, 641-646.

Orghidan, T., 1959. Ein neuer Lebensraum des unterirdischen Wassers: der hyporheische Biotop, *Arch. Hydrobiol.*, **55**, 392-414.

Osiensky, J. L., Nimmer, R., and Binley, A. M., 2004. Borehole cylindrical noise during hole-surface and hole-hole resistivity measurements, *Journal of Hydrology*, **289**, 78-94.

Paasche, H., Tronicke, J., Holliger, K., Green, A. G., and Maurer, H., 2006. Integration of diverse physical-property models: Subsurface zonation and petrophysical parameter estimation based on fuzzy c-means cluster analyses, *Geophysics*, **71**, H33-H44.

Paasche, H., and Tronicke, J., 2007. Cooperative inversion of 2D geophysical data sets: A zonal approach based on fuzzy c-means cluster analysis, *Geophysics*, **72**, A35-A39.

Paasche, H., Wendrich, A., Tronicke, J., and Trela, C., 2008. Detecting voids in masonry by cooperatively inverting P-wave and georadar traveltimes, *Journal of Geophysics and Engineering*, **5**, 256-267.

Paige, C. C., and Saunders, M. A., 1982. LSQR: An algorithm for sparse linear equations and sparse least squares, *ACM Transactions on Mathematical Software*, **8**, 43-71.

Palmer, M. A., Bernhardt, E. S., Allan, J. D., Lake, P. S., Alexander, G., et al., 2005. Standards for ecologically successful river restoration, *Journal of Applied Ecology*, **42**, 208-217.

Park, S. K., Johnston, M. J. S., Madden, T. R., Morgan, F. D., and Morrison, H. F., 1993. Electromagnetic precursors to earthquakes in the ULF band - a review of observations and mechanisms, *Reviews of Geophysics*, **31**, 117-132.

Parker, R. L., 1984. The inverse problem of resistivity sounding, *Geophysics*, **49**, 2143-2158.

Pasquale, N., Perona, P., Schneider, P., Shrestha, J., Wombacher, A., and Burlando, P., 2011. Modern comprehensive approach to monitor the morphodynamic evolution of a restored river corridor, *Hydrology and Earth System Sciences*, **15**, 1197-1212.

Perrier, F., and Morat, P., 2000. Characterization of electrical daily variations induced by capillary flow in the non-saturated zone, *Pure and Applied Geophysics*, **157**, 785-810.

Petiau, G., 2000. Second generation of lead-lead chloride electrodes for geophysical applications, *Pure and Applied Geophysics*, **157**, 357-382.

Podvin, P., and Lecomte, I., 1991. Finite difference computation of traveltimes in very contrasted velocity models: A massively parallel approach and its associated tools, *Geophysical Journal International*, **105**, 271-284.

Pollock, D., and Cirpka, O. A., 2010. Fully coupled hydrogeophysical inversion of synthetic salt tracer experiments, *Water Resources Research*, **46**, W07501.

Portniaguine, O., and Zhdanov, M. S., 1999. Focusing geophysical inversion images, *Geophysics*, **64**, 874-887.

Pratt, R. G., 1999. Seismic waveform inversion in the frequency domain, part 1: Theory and verification in a physical scale model, *Geophysics*, **64**, 888-901.

Pratt, R. G., and Shipp, R. M., 1999. Seismic waveform inversion in the frequency domain, part 2: Fault delineation in sediments using crosshole data, *Geophysics*, **64**, 902-914.

Pride, S., 1994. Governing equations for the coupled electromagnetics and acoustics of porous-media, *Physical Review B*, **50**, 15678-15696.

Pride, S. R., Berryman, J. G., and Harris, J. M., 2004. Seismic attenuation due to wave-induced flow, *Journal of Geophysical Research-Solid Earth*, **109**, B01201.

Pruess, K., Oldenburg, C. M., and Moridis, G. J., 1999. TOUGH2 user's guide version 2, Rep. LBNL--43134, 204 pp, Lawrence Berkeley National Laboratory.

Ptak, T., and Teutsch, G., 1994. Forced and natural gradient tracer tests in a highly heterogeneous porous aquifer - instrumentation and measurements, *Journal of Hydrology*, **159**, 79-104.

Ramirez, A., Daily, W., Labrecque, D., Owen, E., and Chesnut, D., 1993. Monitoring an underground steam injection process using electrical-resistance tomography, *Water Resources Research*, **29**, 73-87.

Ranguelova, E. B., 2002. *Segmentation of textured images on three-dimensional lattices*: PhD thesis, University of Dublin.

RECORD, 2011. Assessment and modeling of coupled ecological and hydrological dynamics in the restored corridor of the river, *Competence Center Environment and Sustainability*, http://www.cces.ethz.ch/projects/nature/Record.

Regli, C., Rauber, M., and Huggenberger, P., 2003. Analysis of aquifer heterogeneity within a well capture zone, comparison of model data with field experiments: A case study from the river Wiese, Switzerland, *Aquatic Sciences*, **65**, 111-128.

Revil, A., Cathles, L. M., Losh, S., and Nunn, J. A., 1998. Electrical conductivity in shaly sands with geophysical applications, *Journal of Geophysical Research - Solid Earth*, **103**, 23925-23936.

Revil, A., and Cathles, L. M., 1999. Permeability of shaly sands, *Water Resources Research*, **35**, 651-662.

Revil, A., Naudet, V., Nouzaret, J., and Pessel, M., 2003. Principles of electrography applied to self-potential electrokinetic sources and hydrogeological applications, *Water Resources Research*, **39**, 1114.

Revil, A., and Leroy, P., 2004. Constitutive equations for ionic transport in porous shales, *Journal of Geophysical Research-Solid Earth*, **109**, B03208.

Revil, A., and Linde, N., 2006. Chemico-electromechanical coupling in microporous media, *Journal of Colloid and Interface Science*, **302**, 682-694.

Revil, A., Linde, N., Cerepi, A., Jougnot, D., Matthai, S., and Finsterle, S., 2007. Electrokinetic coupling in unsaturated porous media, *Journal of Colloid and Interface Science*, **313**, 315-327.

Revil, A., Trolard, F., Bourrie, G., Castermant, J., Jardani, A., and Mendonca, C. A., 2009. Ionic contribution to the self-potential signals associated with a redox front, *Journal of Contaminant Hydrology*, **109**, 27-39.

Rizzo, E., Suski, B., Revil, A., Straface, S., and Troisi, S., 2004. Self-potential signals associated with pumping tests experiments, *Journal of Geophysical Research-Solid Earth*, **109**, B10203.

Robinson, D. A., Binley, A., Crook, N., Day-Lewis, F. D., Ferre, T. P. A., et al., 2008. Advancing process-based watershed hydrological research using near-surface geophysics: A vision for, and review of, electrical and magnetic geophysical methods, *Hydrological Processes*, **22**, 3604-3635.

Rubin, Y., and Hubbard, S. S. (Eds.), 2005. *Hydrogeophysics*, Springer, Dordrecht, The Netherlands.

Rücker, C., Günther, T., and Spitzer, K., 2006. Three-dimensional modelling and inversion of dc resistivity data incorporating topography - I. Modelling, *Geophysical Journal International*, **166**, 495-505.

Ruelleu, S., Moreau, F., Bour, O., Gapais, D., and Martelet, G., 2010. Impact of gently dipping discontinuities on basement aquifer recharge: An example from Ploemeur (Brittany, France), *Journal of Applied Geophysics*, **70**, 161-168.

Samaritani, E., Shrestha, J., Fournier, B., Frossard, E., Gillet, F., et al., 2011. Heterogeneity of soil carbon pools and fluxes in a channelized and a restored floodplain section (Thur River, Switzerland), *Hydrology and Earth System Sciences Discussions*, **8**, 1059-1091.

Sambridge, M., Braun, J., and Mcqueen, H., 1995. Geophysical parametrization and interpolation of irregular data using natural neighbors, *Geophysical Journal International*, **122**, 837-857.

Sandberg, S. K., Slater, L. D., and Versteeg, R., 2002. An integrated geophysical investigation of the hydrogeology of an anisotropic unconfined aquifer, *Journal of Hydrology*, **267**, 227-243.

Saracco, G., Labazuy, P., and Moreau, F., 2004. Localization of self-potential sources in volcano-electric effect with complex continuous wavelet transform and electrical tomography methods for an active volcano, *Geophysical Research Letters*, **31**, L12610.

Schälchli, U., 1992. The clogging of coarse gravel river beds by fine sediment, *Hydrobiologia*, **235-236**, 189-197.

Schälchli, U., 2008. Geschiebehaushalt im Thurgebiet, *Wasser Energie Luft*, **100**, 23-28.

Schäppi, B., Perona, P., Schneider, P., and Burlando, P., 2010. Integrating river cross section measurements with digital terrain models for improved flow modelling applications, *Computers & Geosciences*, **36**, 707-716.

Scheibe, T. D., and Chien, Y. J., 2003. An evaluation of conditioning data for solute transport prediction, *Ground Water*, **41**, 128-141.

Schmidt, C., Bayer-Raich, M., and Schirmer, M., 2006. Characterization of spatial heterogeneity of groundwater-stream water interactions using multiple depth streambed temperature measurements at the reach scale, *Hydrology and Earth System Sciences*, **10**, 849-859.

Schmidt, C., Conant, B., Bayer-Raich, M., and Schirmer, M., 2007. Evaluation and field-scale application of an analytical method to quantify groundwater discharge using mapped streambed temperatures, *Journal of Hydrology*, **347**, 292-307.

Schneider, P., Vogt, T., Schirmer, M., Doetsch, J., Linde, N., et al., 2011. Towards improved instrumentation for assessing river-groundwater interactions in a restored river corridor, *Hydrology and Earth System Sciences*, **15**, 2531-2549.

Schön, J. H., 1996. *Physical properties of rocks: Fundamentals and principles of petrophysics*, Elsevier Science Publishing Company, Inc.

Schulmeister, M. K., Butler, J. J., Healey, J. M., Zheng, L., Wysocki, D. A., and McCall, G. W., 2003. Direct-push electrical conductivity logging for high-resolution hydrostratigraphic characterization, *Ground Water Monitoring and Remediation*, **23**, 52-62.

Schwarzenbach, R. P., and Westall, J., 1981. Transport of non-polar organic-compounds from surface-water to groundwater - Laboratory sorption studies, *Environmental Science & Technology*, **15**, 1360-1367.

Schwarzenbach, R. P., Giger, W., Hoehn, E., and Schneider, J. K., 1983. Behavior of organic-compounds during infiltration of river water to groundwater - Field studies, *Environmental Science & Technology*, **17**, 472-479.

Schwarzenbach, R. P., Escher, B. I., Fenner, K., Hofstetter, T. B., Johnson, C. A., et al., 2006. The challenge of micropollutants in aquatic systems, *Science*, **313**, 1072-1077.

Seiz, G., and Foppa, N., 2007. Nationales Klima-Beobachtungssystem (GCOS Schweiz), *Bundesamt für Meteorologie und Klimatologie, MeteoSchweiz und ProClim, Bern, Switzerland*.

Selker, J. S., Thevenaz, L., Huwald, H., Mallet, A., Luxemburg, W., et al., 2006. Distributed fiber-optic temperature sensing for hydrologic systems, *Water Resources Research*, **42**, W12202.

Sen, P. N., Scala, C., and Cohen, M. H., 1981. A self-similar model for sedimentary-rocks with application to the dielectric-constant of fused glass-beads, *Geophysics*, **46**, 781-795.

Shankar, V., Eckert, P., Ojha, C. S. P., and Konig, C. M., 2009. Transient three-dimensional modeling of riverbank filtration at Grind well field, Germany, *Hydrogeology Journal*, **17**, 321-326.

Sheffer, M. R., and Oldenburg, D. W., 2007. Three-dimensional modelling of streaming potential, *Geophysical Journal International*, **169**, 839-848.

Sill, W. R., 1983. Self-potential modeling from primary flows, *Geophysics*, **48**, 76-86.

Silliman, S. E., and Booth, D. F., 1993. Analysis of time-series measurements of sediment temperature for identification of gaining vs losing portions of Juday-Creek, Indiana, *Journal of Hydrology*, **146**, 131-148.

Singha, K., and Gorelick, S. M., 2005. Saline tracer visualized with three-dimensional electrical resistivity tomography: Field-scale spatial moment analysis, *Water Resources Research*, **41**, W05023.

Sjödahl, P., Dahlin, T., and Johansson, S., 2009. Embankment dam seepage evaluation from resistivity monitoring data, *Near Surface Geophysics*, **7**, 463-474.

Slater, L., and Sandberg, S. K., 2000. Resistivity and induced polarization monitoring of salt transport under natural hydraulic gradients, *Geophysics*, **65**, 408-420.

Slater, L., Binley, A. M., Daily, W., and Johnson, R., 2000. Cross-hole electrical imaging of a controlled saline tracer injection, *Journal of Applied Geophysics*, **44**, 85-102.

Slater, L., and Binley, A., 2006. Synthetic and field-based electrical imaging of a zerovalent iron barrier: Implications for monitoring long-term barrier performance, *Geophysics*, **71**, B129-B137.

Slob, E., Sato, M., and Olhoeft, G., 2010. Surface and borehole ground-penetrating-radar developments, *Geophysics*, **75**, A103-A120.

Smith, D. G., and Jol, H. M., 1992. Ground-penetrating radar investigation of a Lake Bonneville delta, Provo level, Brigham City, Utah, *Geology*, **20**, 1083-1086.

Soar, P. J., and Thorne, C. R., 2001. *Channel restoration design for meandering rivers*, U.S. Army Engineer Research and Development Center, Vicksburg, Miss.

Spillmann, T., Maurer, H., Willenberg, H., Evans, K. F., Heincke, B., and Green, A. G., 2007. Characterization of an unstable rock mass based on borehole logs and diverse borehole radar data, *Journal of Applied Geophysics*, **61**, 16-38.

Springer, R. K., and Gelhar, L. W., 1991. Characterization of large-scale aquifer heterogeneity in glacial outwash by analysis of slug tests with oscillatory response, *US Geological Survey, Cape Cod*, Report 91-4034.

Stanford, J. A., and Ward, J. V., 1988. The hyporheic habitat of river ecosystems, *Nature*, **335**, 64-66.

Stanford, J. A., and Ward, J. V., 1993. An ecosystem perspective of alluvial rivers - connectivity and the hyporheic corridor, *Journal of the North American Benthological Society*, **12**, 48-60.

Stauffer, F., and Dracos, T., 1986. Experimental and numerical study of water and solute infiltration in layered porous-media, *Journal of Hydrology*, **84**, 9-34.

Storey, R. G., Howard, K. W. F., and Williams, D. D., 2003. Factors controlling riffle-scale hyporheic exchange flows and their seasonal changes in a gaining stream: A three-dimensional groundwater flow model, *Water Resources Research*, **39**, 1034.

Streich, R., van der Kruk, J., and Green, A. G., 2006. Three-dimensional multicomponent georadar imaging of sedimentary structures, *Near Surface Geophysics*, **4**, 39-48.

Streich, R., and van der Kruk, J., 2007a. Accurate imaging of multicomponent GPR data based on exact radiation patterns, *Ieee Transactions on Geoscience and Remote Sensing*, **45**, 93-103.

Streich, R., and van der Kruk, J., 2007b. Characterizing a GPR antenna system by near-field electric field measurements, *Geophysics*, **72**, A51-A55.

Stummer, P., Maurer, H., and Green, A. G., 2004. Experimental design: Electrical resistivity data sets that provide optimum subsurface information, *Geophysics*, **69**, 120-139.

Suski, B., Revil, A., Titov, K., Konosavsky, P., Voltz, M., et al., 2006. Monitoring of an infiltration experiment using the self-potential method, *Water Resources Research*, **42**, W08418.

SVGW, 2004. Jahrbuch 2003/2004, *SVGW, Zürich*.

SVGW, 2007. Empfehlungen – Revitalisierung im Einflussbereich von Trinkwasserfassungen, *Zürich, Switzerland*.

Talley, J., Baker, G. S., Becker, M. W., and Beyrle, N., 2005. Four dimensional mapping of tracer channelization in subhorizontal bedrock fractures using surface ground penetrating radar, *Geophysical Research Letters*, **32**, L04401.

Tarantola, A., 1984a. Inversion of seismic-reflection data in the acoustic approximation, *Geophysics*, **49**, 1259-1266.

Tarantola, A., 1984b. Linearized inversion of seismic-reflection data, *Geophysical Prospecting*, **32**, 998-1015.

Tarantola, A., 1986. A strategy for nonlinear elastic inversion of seismic-reflection data, *Geophysics*, **51**, 1893-1903.

Thony, J. L., Morat, P., Vachaud, G., and LeMouel, J. L., 1997. Field characterization of the relationship between electrical potential gradients and soil water flux, *Comptes Rendus De L'Academie Des Sciences*, **325**, 317-321.

Topp, G. C., Davis, J. L., and Annan, A. P., 1980. Electromagnetic determination of soil-water content - Measurements in coaxial transmission-lines, *Water Resources Research*, **16**, 574-582.

Topp, G. C., Davis, J. L., and Annan, A. P., 1982. Electromagnetic determination of soil-water content using TDR 2. Evaluation of installation and configuration of parallel transmission-lines, *Soil Science Society of America Journal*, **46**, 678-684.

Torrence, C., and Compo, G. P., 1998. A practical guide to wavelet analysis, *Bulletin of the American Meteorological Society*, **79**, 61-78.

Touchard, F., 1999. *Caractérisation hydrogéologique d'un aquifère en socle fracture. Site de Ploëmeur (Morbihan)*: PhD thesis, University of Rennes I.

Trefry, M. G., and Muffels, C., 2007. Feflow: A finite-element ground water flow and transport modeling tool, *Ground Water*, **45**, 525-528.

Triska, F. J., Kennedy, V. C., Avanzino, R. J., Zellweger, G. W., and Bencala, K. E., 1989. Retention and transport of nutrients in a 3rd-order stream in Northwestern California - hyporheic processes, *Ecology*, **70**, 1893-1905.

Triska, F. J., Duff, J. H., and Avanzino, R. J., 1993a. Patterns of hydrological exchange and nutrient transformation in the hyporheic zone of a gravel-bottom stream - examining terrestrial aquatic linkages, *Freshwater Biology*, **29**, 259-274.

Triska, F. J., Duff, J. H., and Avanzino, R. J., 1993b. The role of water exchange between a stream channel and its hyporheic zone in nitrogen cycling at the terrestrial aquatic interface, *Hydrobiologia*, **251**, 167-184.

Tronicke, J., Dietrich, P., Wahlig, U., and Appel, E., 2002. Integrating surface georadar and crosshole radar tomography: A validation experiment in braided stream deposits, *Geophysics*, **67**, 1516-1523.

Tronicke, J., and Holliger, K., 2004. Effects of gas- and water-filled boreholes on the amplitudes of crosshole georadar data as inferred from experimental evidence, *Geophysics*, **69**, 1255-1260.

Tronicke, J., Holliger, K., Barrash, W., and Knoll, M. D., 2004. Multivariate analysis of cross-hole georadar velocity and attenuation tomograms for aquifer zonation, *Water Resources Research*, **40**, W01519.

Trubilowicz, J., Cai, K., and Weiler, M., 2009. Viability of motes for hydrological measurement, *Water Resources Research*, **45**, W00D22.

Trush, W. J., McBain, S. M., and Leopold, L. B., 2000. Attributes of an alluvial river and their relation to water policy and management, *Proceedings of the National Academy of Sciences of the United States of America*, **97**, 11858-11863.

Tryggvason, A., Rögnvaldsson, S. T., and Flóvenz, Ó. G., 2002. Three-dimensional imaging of the P- and S-wave velocity structure and earthquake locations beneath Southwest Iceland, *Geophysical Journal International*, **151**, 848-866.

Tryggvason, A., and Linde, N., 2006. Local earthquake (LE) tomography with joint inversion for P- and S-wave velocities using structural constraints, *Geophysical Research Letters*, **33**, L07303.

Tryggvason, A., and Bergman, B., 2006. A traveltime reciprocity discrepancy in the Podvin & Lecomte time3d finite difference algorithm, *Geophysical Journal International*, **165**, 432-435.

Tsoflias, G. P., Halihan, T., and Sharp, J. M., 2001. Monitoring pumping test response in a fractured aquifer using ground-penetrating radar, *Water Resources Research*, **37**, 1221-1229.

Tsoflias, G. P., and Becker, M. W., 2008. Ground-penetrating-radar response to fracture-fluid salinity: Why lower frequencies are favorable for resolving salinity changes, *Geophysics*, **73**, J25-J30.

Tubino, M., and Seminara, G., 1990. Free forced interactions in developing meanders and suppression of free bars, *Journal of Fluid Mechanics*, **214**, 131-159.

Tufenkji, N., Ryan, J. N., and Elimelech, M., 2002. The promise of bank filtration, *Environmental Science & Technology*, **36**, 422A-428A.

Turesson, A., 2006. Water content and porosity estimated from ground-penetrating radar and resistivity, *Journal of Applied Geophysics*, **58**, 99-111.

van Genuchten, M. T., 1980. A closed-form equation for predicting the hydraulic conductivity of unsaturated soils, *Soil Science Society of America Journal*, **44**, 892-898.

Vasco, D. W., Peterson, J. E., and Majer, E. L., 1995. Beyond ray tomography - Wavepaths and fresnel volumes, *Geophysics*, **60**, 1790-1804.

Vereecken, H., Binley, A., Cassiani, G., Revil, A., and Titov, K. (Eds.), 2006. *Applied hydrogeophysics*, Springer, Dordrecht, The Netherlands.

Vereecken, H., Huisman, J. A., Bogena, H., Vanderborght, J., Vrugt, J. A., and Hopmans, J. W., 2008. On the value of soil moisture measurements in vadose zone hydrology: A review, *Water Resources Research*, **44**, W00D06.

Vogt, T., Hoehn, E., Schneider, P., and Cirpka, O. A., 2009. Untersuchung der Flusswasserinfiltration in voralpinen Schottern mittels Zeitreihenanalyse, *Grundwasser*, **14**, 179-194.

Vogt, T., Schneider, P., Hahn-Woernle, L., and Cirpka, O. A., 2010a. Estimation of seepage rates in a losing stream by means of fiber-optic high-resolution vertical temperature profiling, *Journal of Hydrology*, **380**, 154-164.

Vogt, T., Hoehn, E., Schneider, P., Freund, A., Schirmer, M., and Cirpka, O. A., 2010b. Fluctuations of electrical conductivity as a natural tracer for bank filtration in a losing stream, *Advances in Water Resources*, **33**, 1296-1308.

von Gunten, H. R., Karametaxas, G., and Keil, R., 1994. Chemical Processes in Infiltrated Riverbed Sediments, *Environmental Science & Technology*, **28**, 2087-2093.

von Gunten, U., and Zobrist, J., 1993. Biogeochemical changes in groundwater-infiltration systems - column studies, *Geochimica Et Cosmochimica Acta*, **57**, 3895-3906.

Vozoff, K., and Jupp, D. L. B., 1975. Joint inversion of geophysical data, *Geophysical Journal of the Royal Astronomical Society*, **42**, 977-991.

Ward, A. S., Gooseff, M. N., and Singha, K., 2010. Imaging hyporheic zone solute transport using electrical resistivity, *Hydrological Processes*, **24**, 948-953.

Ward, J. V., 1989. The four-dimensional nature of lotic ecosystems, *Journal of the North American Benthological Society*, **8**, 2-8.

Watanabe, T., Nihei, K. T., Nakagawa, S., and Myer, L. R., 2004. Viscoacoustic wave form inversion of transmission data for velocity and attenuation, *Journal of the Acoustical Society of America*, **115**, 3059-3067.

Waxman, M. H., and Smits, L. J. M., 1968. Electrical Conductivities in Oil-Bearing Shaly Sands, *Society of Petroleum Engineers Journal*, **8**, 107.

West, L. J., Handley, K., Huang, Y., and Pokar, M., 2003. Radar frequency dielectric dispersion in sandstone: Implications for determination of moisture and clay content, *Water Resources Research*, **39**, 1026.

Western, A. W., Grayson, R. B., and Blöschl, G., 2002. Scaling of soil moisture: A hydrologic perspective, *Annual Review of Earth and Planetary Sciences*, **30**, 149-180.

Wilkinson, P. B., Meldrum, P. I., Kuras, O., Chambers, J. E., Holyoake, S. J., and Ogilvy, R. D., 2010. High-resolution electrical resistivity tomography monitoring of a tracer test in a confined aquifer, *Journal of Applied Geophysics*, **70**, 268-276.

Winship, P., Binley, A., and Gomez, D., 2006. Flow and transport in the unsaturated Sherwood Sandstone: Characterization using cross-borehole geophysical methods, *Fluid Flow and Solute Movement in Sandstones: The Onshore UK Permo-Triassic Red Bed Sequence*, **263**, 219-231.

Wishart, D. N., Slater, L. D., and Gates, A. E., 2006. Self potential improves characterization of hydraulically-active fractures from azimuthal geoelectrical measurements, *Geophysical Research Letters*, **33**, L17314.

Woessner, W. W., 2000. Stream and fluvial plain ground water interactions: Rescaling hydrogeologic thought, *Ground Water*, **38**, 423-429.

Wombacher, A., and Schneider, P., 2010. Observation centric sensor data model, *Technical Report TR-CTIT-10-13, University of Twente, Enschede*, ISSN 1381-3625.

Woolsey, S., Capelli, F., Gonser, T., Hoehn, E., Hostmann, M., et al., 2007. A strategy to assess river restoration success, *Freshwater Biology*, **52**, 752-769.

Worthington, P. F., 1993. The uses and abuses of the archie equations 1. The formation factor porosity relationship, *Journal of Applied Geophysics*, **30**, 215-228.

Wriedt, G., and Rode, M., 2006. Modelling nitrate transport and turnover in a lowland catchment system, *Journal of Hydrology*, **328**, 157-176.

Wroblicky, G. J., Campana, M. E., Valett, H. M., and Dahm, C. N., 1998. Seasonal variation in surface-subsurface water exchange and lateral hyporheic area of two stream-aquifer systems, *Water Resources Research*, **34**, 317-328.

Yeh, T. C. J., Liu, S., Glass, R. J., Baker, K., Brainard, J. R., et al., 2002. A geostatistically based inverse model for electrical resistivity surveys and its applications to vadose zone hydrology, *Water Resources Research*, **38**, 1278.

Yeh, T. C. J., Lee, C. H., Hsu, K. C., Illman, W. A., Barrash, W., et al., 2008. A view toward the future of subsurface characterization: CAT scanning groundwater basins, *Water Resources Research*, **44**, W03301.

Yilmaz, Ö., 2001. *Seismic data processing*, Society of Exploration Geophysicists, Tulsa, USA.

Zhang, J., and Morgan, F. D., 1997. Joint Seismic and Electrical Tomography, *Proceedings of the Symposium on the Application of Geophysics to Engineering and Environmental Problems*, 391-396.

Zhdanov, M. S., 2009. New advances in regularized inversion of gravity and electromagnetic data, *Geophysical Prospecting*, **57**, 463-478.

Zhou, B., and Greenhalgh, S. A., 2003. Crosshole seismic inversion with normalized full-waveform amplitude data, *Geophysics*, **68**, 1320-1330.

Zonge, K., Wynn, J., and Urquhart, S., 2005. Resistivity, induced polarization, and complex resistivity, in *Near Surface Geophysics*, edited by D. K. Butler, pp. 265-300, SEG.

Zurbuchen, B. R., Zlotnik, V. A., and Butler, J. J., 2002. Dynamic interpretation of slug tests in highly permeable aquifers, *Water Resources Research*, **38**, 1025.